Title

Gli1$^+$ mesenchymal stromal cells form a pathological niche to promote airway progenitor metaplasia in the fibrotic lung.

Authors

Cassandras, Monica
Wang, Chaoqun
Kathiriya, Jaymin
et al.

Gli1+ mesenchymal stromal cells form a pathological niche to promote airway progenitor metaplasia in the fibrotic lung

Monica Cassandras[1], **Chaoqun Wang**[1], **Jaymin Kathiriya**[1], **Tatsuya Tsukui**[1], **Peri Matatia**[2], **Michael Matthay**[1], **Paul Wolters**[1], **Ari Molofsky**[2], **Dean Sheppard**[1], **Hal Chapman**[1], **Tien Peng**[1,*]

[1]Department of Medicine, Division of Pulmonary and Critical Care Medicine, Cardiovascular Research Institute

[2]Department of Laboratory Medicine, University of California San Francisco, San Francisco, CA 94143

Abstract

Aberrant epithelial reprogramming can induce metaplastic differentiation at sites of tissue injury, culminating in transformed barriers composed of scar and metaplastic epithelium. While the plasticity of epithelial stem cells is well-characterized, the identity and role of the niche has not been delineated in metaplasia. Here we show that *Gli1+* mesenchymal stromal cells (MSCs), previously shown to contribute to myofibroblasts during scarring, promote metaplastic differentiation of airway progenitors into KRT5+ basal cells. During fibrotic repair, *Gli1+* MSCs integrate hedgehog activation to upregulate BMP antagonism in the progenitor niche that promotes metaplasia. Restoring the balance towards BMP activation attenuated metaplastic KRT5+ differentiation while promoting adaptive alveolar differentiation into SFTPC+ epithelium. Finally, fibrotic human lungs demonstrate altered BMP activation in the metaplastic epithelium. These findings show that *Gli1+* MSCs integrate hedgehog signaling as a rheostat to control BMP activation in the progenitor niche to determine regenerative outcome in fibrosis.

Main

A canonical feature of wound repair is the formation of scar tissue, composed of inflammatory cells and resident mesenchymal subsets that dynamically remodel the wound to close any barrier gaps. Scars are sometimes accompanied by epithelial metaplasia, defined as interconversion of one mature cell type into another that is not typically present at the site

*Address correspondence to: Tien Peng, M.D., University of California, San Francisco, 513 Parnassus Ave., HSE Building, Room 1312, Box 0130, San Francisco, CA 94143, tien.peng@ucsf.edu.

Author Contributions

M.C. and T.P. conceived the experiments. M.C., C.W., J.K., T.T., P.M., M.M., and P.W. performed the experiments and data analysis. D.S., A.M., and H.C. provided expertise and feedback. M.C. and T.P. wrote the manuscript.

Code Availability

This study does not include any custom code.

of injury[1]. One of the cardinal features of idiopathic pulmonary fibrosis (IPF), the most prevalent and deadly subtype of progressive fibrotic lung diseases, is the appearance of "bronchiolization" on histology[2]. This pathological feature denotes the ectopic appearance of proximal bronchus/airway epithelium within the distal lung, characterized by metaplastic KRT5+ basal cells lining cystic airspaces in the alveoli alongside patches of fibroblastic scars[3,4]. While the functional relationship between metaplasia and scarring is unclear in IPF, the appearance of metaplastic KRT5+ cells is correlated with worsening disease severity and survival[5]. This suggests that epithelial metaplasia is a clinically relevant feature of organ fibrosis and a potential therapeutic target.

The lung is populated by unique resident epithelial stem/progenitor cells along the proximal-distal axis. KRT5+ basal cells reside in the trachea and large airways in the murine lung, and SFTPC+ Type 2 cells reside in the distal alveolar sacs to generate functional alveolar epithelium[6]. In recent years, numerous studies have shown that KRT5-negative progenitors from the airway can migrate and reconstitute epithelium in the alveoli in response to severe damage[7–10]. While the heterogeneity within this airway progenitor population (EpCAM+ cells expressing combinations of *Sox2*, *tp63*, *Scgb1a1*, and *Itgb4*) has not been fully resolved, genetic lineage tracing and transplant experiments clearly demonstrate that KRT5-negative airway progenitors can replete the damaged alveolar surface with endogenous (SFTPC+) or metaplastic (KRT5+) epithelium with significant functional consequences depending on the regenerative outcome.

Gli1, a transcriptional readout of hedgehog (Hh) activation, labels mesenchymal cells adjacent to the airway epithelium[11]. *Gli1*+ cells have been demonstrated to exhibit properties of mesenchymal stromal cells (MSCs) *ex vivo*[12–14], and contribute to fibrotic scarring in the lung and other organs through differentiation into myofibroblasts and secretion of collagen[14]. We have previously demonstrated that ectopic activation of hedgehog in the alveolar mesenchyme disrupts SFTPC+ alveolar progenitor renewal during homeostasis[15]. In this study, we set out to define the functional interactions between the *Gli1*+ niche cells and metaplastic differentiation of airway epithelial progenitors in the fibrotic lung.

Results

Gli1+ mesenchymal cells promote metaplastic KRT5 differentiation from the airway

SOX2+ progenitors are normally restricted to the airway epithelium during homeostasis, but they migrate into the alveoli during severe alveolar damage from influenza[7,16]. To determine whether SOX2+ progenitors have similar migratory capacity in a fibrotic model, we adapted a repetitive bleomycin model of lung fibrosis that better captured features of IPF compared to the single dose model, including the appearance of cystic airspaces and metaplastic basal cells in the alveoli (Extended Data Fig. 1a,b)[17,18]. Our genetic lineage tracing confirms that *Sox2* lineage traced (*Sox2* Lin+) airway progenitors expand and differentiate into metaplastic KRT5+/SOX2+ or endogenous SFTPC+/SOX2-epithelium in the alveoli in this model of severe fibrotic injury (Fig. 1a,b, ED Fig. 1c,d). Fidelity of the *Sox2^creERT2* driver was validated by SOX2 antibody staining of tamoxifen and corn oil controls (ED Fig. 1e–g). Interestingly, *p63* Lin+ airway progenitors, previously found to contribute to KRT5+ basal

cells after influenza infection[9], did not contribute significantly to alveolar KRT5+ basal cells after bleomycin (ED. Fig 2a–d). In contrast, *Scgb1a1* Lin+ airway progenitors which co-express *Sox2*[7], contributes to a significant proportion of alveolar basal cells after bleomycin (ED Fig. 2e,f).

Immunofluorescence of *Gli1* lineage-labeled cells (*Gli1* Lin+) demonstrates that they are localized right beneath the basement membrane in close proximity to SOX2+ airway epithelium (Fig. 1c,d) during normal homeostasis. *Gli1* Lin+ mesenchymal cells also respond to fibrotic injury by migrating into the alveolar compartment (Fig. 1e, ED Fig. 3d). Fidelity of *Gli1*^{creERT2} driver was validated by corn oil controls and comparable Gli1 reporter (ED Fig. 3a–c). Cell-to-cell distance quantification shows that the ectopic SOX2+ cells in the alveoli maintain a close distance to *Gli1* Lin+ cells that migrated into the alveoli (Fig.1f), suggesting a functional interaction between migratory *Gli1* Lin+ mesenchyme and SOX2+ progenitors as niche partners during repair.

To determine whether *Gli1*+ mesenchymal cells are required for metaplastic KRT5 differentiation in the alveoli, we genetically deleted *Gli1*+ cells by inducible expression of diphtheria toxin A (DTA) within *Gli1*-expressing cells and evaluated airway progenitor differentiation as previously described[8,15,16]. Tamoxifen induction of *Gli1*$^{creERT/+}$:*R26*$^{DTA/DTA}$ (*Gli1*-deleted) animals alone without injury did not change the composition of the airway epithelium (ED Fig. 3f,g). Tamoxifen induction of *Gli1*-deleted animals followed by repetitive bleomycin resulted in significantly reduced areas of metaplastic KRT5+ pods on histology compared to control *R26*$^{DTA/DTA}$ animals, and a higher proportion of alveolar epithelium marked by the Type 2 cell marker, SFTPC (Fig. 1g,h), along with a trend toward decrease in fibrotic markers (ED Fig. 3j). This suggests that activated *Gli1*+ mesenchymal cells form a pathological niche to promote metaplastic differentiation after fibrotic injury.

To determine the ability of *Gli1*+ mesenchymal cells to modify airway progenitors *in vitro*, we co-cultured airway progenitors isolated from the lung (separated from the trachea) with or without *Gli1*+ mesenchymal cells in a heterotypic 3D organoid assay[15] (Fig. 2a, ED Fig. 4c). Cytospin confirmed that ITGB4-sorted lung epithelium largely overlaps with SOX2, with minimal KRT5 or SFTPC-expressing cells (ED Fig. 4a,b). ITGB4+ progenitors cultured without mesenchyme failed to form organoids, but co-culture of ITGB4+ airway progenitors with *Gli1*+ mesenchyme resulted in significant growth in the 3D matrigel (Fig. 2b,c). Histologic analysis of the organoids co-cultured with *Gli1*+ cells demonstrated heterogeneous lineage differentiation that included organoids containing either KRT5+ or SFTPC+ cells, but never both in the same organoid (Fig. 2d). To ensure that the newly formed KRT5+ or SFTPC+ cells did not arise from pre-existing KRT5+ or SFTPC+ cells in the ITGB4 sort, we isolated ITGB4+ progenitors from lungs of *Krt5* or *Sftpc* lineage-traced lungs for co-culture with *Gli1*+ mesenchyme, and immunophenotyping showed that <5% of the KRT5+ or SFTPC+ cells in the organoids were *Krt5* or *Sftpc* Lin+ respectively (ED Fig. 4d–j). We next isolated *Gli1* Lin+ or Lin- mesenchyme from PBS or bleomycin-treated lungs for co-culture with healthy ITGB4+ airway progenitors (Fig. 2e), which demonstrated that *Gli1* Lin+ mesenchyme increased the colony forming efficiency (CFE) of airway progenitors in both uninjured and injured lungs compared to *Gli1* Lin- mesenchyme (Fig.

2f,g). Lastly, immunophenotyping of the organoids containing *Gli1* Lin+ mesenchyme shows that bleomycin injury in the mesenchyme significantly increases the proportion of KRT5+ basal cell organoids with a trend towards reduction in SFTPC+ organoids when compared to PBS-treated *Gli1* Lin+ mesenchyme (Fig. 2h). This demonstrates that *Gli1*+ mesenchyme forms a niche to support airway progenitor expansion and differentiation *in vitro*.

Mesenchymal Hh activation promotes metaplastic KRT5 differentiation

Gli1+ mesenchyme integrates extracellular cues during normal homeostasis and repair, including the availability of the SHH ligand that modulates the level of Hh activation in the tissue microenvironment[11]. Analysis of *Shh* expression during bleomycin injury shows expression in the ectopic SOX2+ airway progenitors that migrate into the alveoli (ED Fig. 5a). To determine the role of mesenchymal Hh activation as a niche signal modulating airway progenitor differentiation, we inducibly expressed a constitutively active form of the Hh effector, *Smo* (*SmoM2*), in *Gli1*+ cells[19]. Over-activation of Hh in *Gli1*+ mesenchyme through tamoxifen induction of *Gli1*$^{creERT/+}$:*R26*$^{SmoM2/YFP}$ (referred to as Hh-activated) animals did not induce metaplastic differentiation in the uninjured lung (ED Fig. 5b,c). However, when Hh over-activation is followed by fibrotic injury with bleomycin, Hh-activated animals demonstrated a significant increase in areas of the lung with metaplastic KRT5+ basal cells along with a significantly reduced proportion of functional SFTPC+ alveolar epithelium compared to controls (Fig. 3a,b). We then performed genetic deletion of *Smo* using *Gli1*$^{creERT/+}$:*Smo*$^{fl/fl}$ animals treated with either corn oil (control) or tamoxifen (Hh-inactivated) followed by injury. Hh-inactivation in *Gli1*+ mesenchyme attenuated KRT5+ metaplasia and increased SFTPC+ cells in the alveoli, along with an improvement in gas exchange as shown by oximetry (Fig. 3c–e). Surprisingly, Hh activation in *Gli1* Lin+ cells followed by fibrosis did not increase the number of *Gli1* Lin+ cells in the alveoli, with a trend towards an increase in myofibroblastic differentiation (ED Fig. 5d–f). This data shows that Hh activation within *Gli1*+ mesenchyme, in conjunction with a fibrotic stimulus, acts in trans to promote the metaplastic differentiation in the airway progenitor niche.

To determine whether mesenchymal Hh activation *in vivo* promotes the differentiation of isolated airway progenitors *in vitro*, we isolated injured control or Hh-activated *Gli1* Lin+ lung mesenchyme with healthy ITGB4+ airway progenitors in our organoid assay (Fig. 3f). Hh-activated *Gli1* Lin+ mesenchyme increased the CFE of airway progenitors and increased KRT5+ basal cell organoids at the expense of SFTPC+ organoids compared to control mesenchyme (Fig. 3g–i). To activate Hh in the lung mesenchyme *in vitro*, we first generated a transgenic animal (*Ubc*$^{creERT2/+}$:*R26*$^{SmoM2/+}$) where constitutively active *SmoM2* could be induced in isolated lung mesenchymal cells *in vitro* utilizing a *creERT2* allele driven by a ubiquitously expressing promoter as previously described[11,15]. We activated Hh in isolated lung mesenchyme by addition of 4-hydroxytamoxifen (4OHT), followed by co-culture with wild type ITGB4+ progenitors in our 3D organoid assay. Activation of Hh in the mesenchyme *in vitro* resulted in appropriate induction of *Gli1* in the separated mesenchyme (ED Fig 5h). Hh activation in the mesenchyme significantly increased the expression of *Krt5* in the epithelial organoids and decreased the expression of *Sftpc* along with similar trends in immunophenotyping of KRT5+ and SFTPC+ organoids (ED Fig. 5i–l). These results

demonstrate that Hh activation of mesenchyme promotes the metaplastic differentiation of airway progenitors into basal cells during fibrotic repair, likely through the alteration of niche factors secreted by *Gli1*+ mesenchyme (Fig. 3j).

Single cell transcriptome analysis of *Gli1*+ mesenchyme reveals upregulated BMP antagonism in the fibrotic niche

To determine transcriptome alterations that could modify *Gli1*+ cells' ability to alter airway progenitor behavior, we performed single cell RNA-sequencing (scRNA-seq) on sorted *Gli1* Lin+ mesenchymal cells before and after fibrotic injury (Fig. 4a). 17,620 cells were captured from lineage labeled *Gli1* Lin+ cells from *Gli1^creERT/+;R26^YFP/YFP* lungs treated with PBS or bleomycin. PBS and bleo-treated datasets were merged and projection of transcriptomic variations of individual cells by Uniform Manifold Approximation and Projection (UMAP)[20] shows three main clusters, defined by their anatomic localization and differentiation (Fig. 4b). Based on our prior study showing that mesenchyme surrounding the airway exhibits distinct identity from those in the alveoli[15], Cluster 1 and Cluster 2 represent the airway and alveolar subsets respectively, whereas Cluster 3 represents a *de novo* population expressing myofibroblast markers that appears only during fibrotic injury in the alveoli (Fig. 4c). Bleomycin-injured *Gli1* Lin+ cells demonstrate an increase in proportion of cells in the alveolar subset (Fig. 4d), and gave rise to the entire myofibroblast subset that generates scarring in the alveoli along with portions of the alveolar subset (Fig. 4d, green box). RNA velocity analysis[21] on *Gli1* Lin+ mesenchymal cells treated with bleomycin predicted two distinct trajectories where airway mesenchymal cells gives rise to either alveolar mesenchymal cells or myofibroblasts during fibrotic repair (Fig. 4e), which is supported by multi-color clonal analysis using the *R26^Confetti* reporter coupled with *Gli1* lineage tracing after bleomycin injury (ED Fig. 6a)

Differential gene expression analysis between *Gli1* Lin+ cells treated with PBS vs. bleomycin showed that *Gli1* Lin+ cells retained *Gli1* expression after injury even as they migrate into the alveoli (ED Fig. 6b). Fibrotic *Gli1* Lin+ mesenchyme upregulated genes classified as "TGF-β signaling components" and "negative regulation of BMP signaling" according to Gene Ontology (GO) analysis (Fig. 4f,g). The upregulation of secreted BMP antagonists, particularly *Grem2* and *Fst*, is most pronounced in the *Gli1* Lin+ cells that appear *de novo* in bleomycin, including the myofibroblast cluster (Fig. 4h). Secreted BMP antagonists are almost exclusively expressed in the mesenchyme of the lung in a publicly available murine lung cellular atlas (Tabula muris)[22]. Additionally, numerous BMP ligands are also expressed in the *Gli1*+ mesenchyme, including *Bmp3, 4, 5,* and *7* (Fig. 4i), with *Bmp7* significantly downregulated in bleomycin treatment. Our single cell analysis suggests that *Gli1* Lin+ mesenchyme upregulates local BMP antagonism during fibrotic repair through the secretion of soluble BMP antagonists in the fibrotic niche.

Hh activation upregulates BMP antagonism in the fibrotic lung

During organ morphogenesis, Hh and BMP signaling are often mutually antagonistic, forming antiparallel gradients of activation within the same tissue to define segmental cell fate[23]. Activation of the BMP receptor leads to intracellular phosphorylation of SMAD1, 5, and 8, which serves as a readout for BMP activation[24]. Quantification of phosphorylated-

SMAD1/5/8 (pSMAD1/5/8) staining in the *Sox2* Lin+ cells in the alveoli after injury shows that the majority of BMP-activated *Sox2* Lin+ cells were SCGB1A1+ or SFTPC+, but rarely KRT5+ (ED Fig. 7a,b). To determine the effect of Hh activation on BMP activation, we quantified the pSMAD1/5/8+ areas in the bleomycin-injured lungs, which showed a reduction of alveolar areas stained by pSMAD1/5/8 in the Hh-activated lungs compared to controls (Fig. 5a,b), suggesting that Hh activation antagonizes BMP activation in fibrotic repair.

Next, we examined the expression of secreted BMP antagonists in the Hh-activated and control lungs treated with bleomycin. Genes encoding soluble BMP antagonists were upregulated in the fibrotic Hh-activated lungs compared to controls by whole lung qPCR analysis (Fig. 5c). These data suggest that Hh activation antagonizes BMP activation during fibrotic repair by upregulating secreted antagonists of BMP signaling in the *Gli1* Lin+ mesenchyme.

To determine whether Hh activation directly upregulates BMP antagonists *in vitro*, we collected Hh-inducible mesenchyme from the $Ubc^{creERT2/+}$:$R26^{SmoM2/+}$ lungs and induced Hh activation with 4OHT (Fig. 4d, ED Fig. 7c). Surprisingly, Hh-activated mesenchyme showed minimal induction of the BMP antagonist, *Grem2*. Recombinant TGF-β1, a fibrotic stimulus upregulated in the fibrotic *Gli1* Lin+ mesenchyme, also had minimal effect on *Grem2* expression when added alone to control lung mesenchyme. However, TGF-β1 activation in conjunction with Hh activation *in vitro* significantly increased the expression of *Grem2* (Fig. 5d), which was the most upregulated BMP antagonists in the Hh-activated lungs *in vivo* (Fig. 5c). This suggests a synergistic interaction between TGF-β and Hh in upregulating BMP antagonism in the fibrotic niche. Conversely, both Hh and TGF-β activation can independently suppress the expression of *Bmp3*, *Bmp4*, *Bmp5*, and *Bmp7* from the mesenchyme, with the most profound effect on *Bmp4* and *Bmp5* when both Hh and TGF-β are activated (Fig. 5d). Hh-activation in the mesenchyme reduced pSMAD1/5/8 staining in the epithelial organoids, along with expression of BMP-target genes *Id1* and *Id2* in the epithelium (Fig. 5e–h). These results demonstrate that Hh activation suppresses BMP activation by simultaneously upregulating soluble BMP antagonists in the mesenchyme and downregulating BMP ligands in the fibrotic niche (Fig. 5i).

BMP activation attenuates metaplastic airway progenitor differentiation

To test whether BMP activation can modify metaplastic KRT5 differentiation *in vivo*, we directly dosed recombinant BMP into the lung undergoing bleomycin treatment. Histologically, injured wild type animals treated with recombinant human BMP4 (rhBMP4) demonstrated a significant reduction in the areas of lung occupied by KRT5+ cystic airspace concurrent with an increase in the proportion of SFTPC+ cells compared to vehicle, along with an improvement in oximetry and fibrotic markers (Fig. 6a–c, ED Fig. 8a–c). One possible side effect of rhBMP4 is the induction of chondrogenic markers in the lung as seen on qPCR (ED Fig. 8e). To determine the lineage origin of the SFTPC+ cells seen in rhBMP4 treated lungs, we repeated the same experiment with *Sox2* lineage traced animals. Quantification of *Sox2* Lin+ cells in the alveoli showed that rhBMP4 increased the proportion of SFTPC+/*Sox2* Lin+ cells with a concurrent reduction in KRT5+/*Sox2* Lin+

cells (Fig. 6d,e), with no difference in the total number of *Sox2* Lin+ cells that migrated into the alveoli (ED Fig. 8f).

To test the effect of BMP modulation in the airway progenitor *in vitro*, we co-cultured ITGB4+ airway progenitors and *Gli1*+ mesenchyme with recombinant BMP4 or BMP antagonist, GREMLIN2, in our 3D organoid assay (ED Fig. 8g). Addition of BMP4 increased the expression of *Sftpc* in the epithelial organoid and reduced the expression of *Krt5*, and GREMLIN2 had the opposite effects (ED Fig. 8i). Furthermore, addition of BMP4 to airway progenitors co-cultured with Hh-activated mesenchyme attenuated KRT5 metaplasia in the organoids (Fig. 6f,g), further supporting that BMP antagonism occurs downstream of Hh-activation to drive KRT5 differentiation. These data demonstrate that BMP activation promotes the differentiation of mobilized airway progenitors into adaptive SFTPC+ alveolar epithelium (Fig. 6h), and the prevention of epithelial metaplasia is physiologically significant for improving gas exchange.

IPF lungs display altered BMP activation in the epithelium

To determine whether fibrotic human lung mesenchyme undergoes similar transcriptomic alterations as seen in the murine *Gli1*+ mesenchyme, we analyzed single cell RNA-sequencing (scRNA-seq) of human lungs from IPF and normal controls (n = 3 per group). The diseased lungs were collected from patients with an established diagnosis of IPF undergoing lung transplantation, and controls were from sex and age-matched cadaveric donor lungs without prior history of lung disease. Mesenchymal cells were segregated based on presence of *Pdgfra* as a mesenchymal marker, with *Pdgfra*+ cells from each lung merged for comparison (Fig. 7a,b, ED Fig. 9a). UMAP analysis shows emergence of cellular subsets in the fibrotic lung that are distinct from *Pdgfra*+ cells from healthy controls (ED Fig. 7b, ED Fig. 9a), with cluster 3 derived almost entirely from IPF lungs and enriched for scar components such as genes associated with myofibroblast differentiation (*ACTA2* and *ASPN*) and matrix deposition (*COL1A1*) (Fig. 7c,d). Differential gene expression of the scRNA-seq dataset with GO analysis shows a significant enrichment of BMP antagonists in the fibrotic human lung mesenchyme compared to normal controls (Fig. 7e,f). Furthermore, the upregulated BMP antagonists demonstrate particular enrichment in the scar-forming fibroblasts (Cluster 3) (Fig. 7g).

Histological analysis of IPF lungs demonstrates areas of intense scarring in the alveoli, marked by the presence of SMA+ fibroblastic foci, which are often localized adjacent to metaplastic KRT5+ cells, neither of which are present in the normal alveoli (Fig. 7h). Similar to mouse, metaplastic KRT5+ basal cells in the alveoli of IPF lungs co-label with SOX2, along with KRT14, NGFR, and p63 (ED Fig. 9b), which are normally markers of airway differentiation in the human lung as well[25]. Cell-to-cell distance quantification of metaplastic SOX2+/KRT5+ cells in the alveoli demonstrates that they are equally proximate to the SMA+ fibroblastic foci when compared to the endogenous SFTPC+ epithelium (ED Fig. 9c,d).

Unlike the mouse lung, KRT5+ basal cells extend more distally in the normal human airway, lining the basal side of the pseudostratified epithelium of the distal airways[6]. Analysis of pSMAD1/5/8 shows intense staining in the airway epithelium of normal lungs, including

uniform expression in the KRT5+ basal cells (Fig. 7i). However, in the IPF lungs, the airway epithelium appears dysplastic, with overgrowth of the SOX2+ epithelium and non-uniform distribution of pSMAD1/5/8 staining within the disorganized KRT5+ basal cell layer (Fig. 7j). Furthermore, metaplastic SOX2+/KRT5+ basal cells in the alveoli demonstrates a significant reduction in pSMAD1/5/8 staining compared to their airway counterparts (Fig. 7j,k), similar to what we observed in the mouse (ED Fig. 7a,b). Finally, unsorted epithelial organoids were cultured from dissociated IPF lungs and treated with BMP4, which significantly attenuated the growth of KRT5+ organoids (ED Fig. 9e,f). This suggests that BMP activation can either attenuate KRT5+ basal cell proliferation, or reduce differentiation into KRT5+ basal cells from a precursor population not yet identified in human lung. This data shows that the fibroblastic scars in IPF upregulate BMP antagonism in the local environment, concurrent with a downregulation of BMP activation in metaplastic KRT5+ cells that appears to be a conserved feature of epithelial metaplasia in lung fibrosis.

Discussion

The ectopic appearance of mature epithelial cell types under pathological settings (*i.e.* metaplasia) is a feature of chronic wounds that often appears at tissue transition zones[1]. Our study demonstrates how a putative MSC population (*Gli1+* mesenchymal cells) that contributes to scarring can form a pathological niche to promote epithelial metaplasia, providing a functional link between two commonly observed pathological phenomena in organ fibrosis. Utilizing temporally and spatially-precise *in vivo* manipulation and *ex vivo* cellular modeling, we show that *Gli1+* mesenchyme integrates Hh activation to modify the extracellular BMP environment, which in turn regulates the metaplastic fate of adjacent airway progenitors in fibrotic repair (ED Fig. 10).

Hh and BMP are key developmental morphogens that often form activation gradients in an antiparallel orientation to generate asymmetric patterning. Cells in the developing foregut and neural tube sense the local balance between Hh and BMP activation that specifies ventral (Hh predominant) vs. dorsal (BMP predominant) fate[23]. While mutual antagonism between Hh and BMP is crucial for morphogenesis, questions remain as to whether and how the two pathways continue to interact in adult tissues during maintenance and repair. In the respiratory system, it has been reported that BMP antagonists are upregulated after injury to the tracheal epithelium, and inhibition of BMP drives basal cell proliferation[26,27]. Our single cell data shows that *Gli1+* mesenchyme is the key source of numerous soluble BMP antagonists, along with BMP ligands that are expressed in the mesenchyme and other cell types. This suggests a cellular microenvironment in the adult lung where the balance between BMP ligands and soluble antagonists is tightly regulated, and Hh controls the secretion of BMP antagonists in *Gli1+* mesenchymal cells to modulate the state of local BMP activation. We have previously shown that Hh maintains airway mesenchymal cell identity[15], but what is surprising about our new data is that Hh also appears to promote airway epithelial cell fate in trans by driving BMP antagonism in the fibrotic progenitor niche. This suggests a mechanism where Hh and BMP continue to compete in adult tissues to segregate compartmental identity during regeneration, by acting through a mesenchymal effector that modifies epithelial cell fate.

Over-activation of Hh has been reported in patients with IPF[28–30], but pharmacologic inhibition of the pathway has produced mixed results in experimental models of lung fibrosis[31,32]. The overwhelming endpoints of these experimental fibrotic studies have been the reduction of scarring, as measured by collagen content in the lungs as a therapeutic endpoint. However, our study demonstrates that epithelial metaplasia is an equally important endpoint in lung fibrosis. We found that administration of rhBMP4 is able to promote the repletion of the alveolar epithelium with endogenous SFTPC+ type 2 cells, which also improved gas exchange as seen in the improved oximetry. While the cellular origin of the ectopic KRT5+ basal cells in human IPF remains unclear, the downregulation of BMP activation in the ectopic alveolar KRT5+ basal cells compared to airway KRT5+ basal cells suggests that BMP could regulate the "bronchiolization" of alveoli, supported by previous studies demonstrating an upregulation of BMP antagonists in lung fibrosis[33–35]. Our study highlights the need for other physiologically-relevant endpoints in experimental fibrosis studies, and suggest that epithelial metaplasia presents both an attractive therapeutic target as well as a clinical endpoint for tissue fibrosis.

Methods

Animal Studies

All animals were housed and treated in compliance with the Institutional Animal Care and Use Committee (IACUC) protocol approved at the University of California, San Francisco. Mice were housed under pathogen-free conditions at room temperature, maintained under standard 12 hour light/dark cycle, and monitored daily by caretakers or researchers. Cage, bedding, and food was changed biweekly. C57BL/6 mice were obtained from Charles River Laboratories. Generation and genotyping of the $Gli1^{EGFP}$, $Gli1^{creERT}$, $Ubc^{creERT2}$, $Sox2^{creERT}$, $Scgb1a1^{creERT}$, $p63^{creERT}$, $SFTPC^{creERT}$, $KRT5^{creERT}$, Smo^{flox}, $Gli1^{LacZ}$, $R26^{SmoM2}$, $R26^{EYFP}$, $R26^{tdTomato}$, $R26^{mTmG}$, $R26^{Confetti}$, and $R26^{DTA}$ lines were performed as previously described by The Jackson Laboratory. For all animal experiments, 6–12 week old littermate male and female mice were gender balanced and randomly assigned to experimental groups. Mice used in experiments were not involved in previous procedures.

Animal Treatment

For lineage tracing studies, tamoxifen (Cat#T5648; Sigma-Aldrich) was dissolved in corn oil and administered intraperitoneally at 200 mg/kg body weight per day for five consecutive days, followed by at least 7 days before bleomycin was administered. For bleomycin injury, mice were given pharmaceutical grade bleomycin (Hospira) dissolved in PBS via intranasal installation once a week for four weeks. Mixed background mice were given a dose of 1 U/kg and C57BL/6 background mice were given 0.75 U/kg per dose. Mice were sacrificed seven days after the final treatment. For BMP4 treatment, mice were treated with 5 μg/mL of human recombinant BMP4 protein in 50μL (Cat#314-BP-010; R&D Systems) via intranasal installation twice a week for four weeks, concurrently with bleomycin injury. Mice were sacrificed seven days after the final bleomycin treatment and two days after the final BMP4 treatment.

Human Lung Tissue

Studies involving human tissue were approved and performed in compliance with the UCSF Institutional Review Board. IPF lungs were obtained from patients independently diagnosed with interstitial pneumonia or scleroderma at the time of lung transplant. Sex and age matched healthy human lungs were provided by the Northern California Donor Network from brain-dead donors in which the lung was independently rejected for transplantation. All subjects provided written informed consent. Samples were collected from all ethnic groups, both male and female patients, and all samples were from patients over 50 years old. Investigators were blind to patient information besides relevant history of lung disease. No patient recruitment was performed for this study.

Histology and Immunofluorescence

The right ventricle of the mice were perfused with 1–3 mL PBS and the lungs were inflated with 1–3 mL 4% paraformaldehyde (PFA) in PBS, and then fixed in 4% PFA overnight at 4 ℃. After fixation, the lungs were washed with cold PBS 4 times for 30 minutes each at 4 ℃, and then dehydrated in a series of increasing ethanol concentration washes (30%, 50%, 70%, 95% and 100%) for a minimum of 2 hours per wash. The dehydrated lungs were incubated with xylene for 1 hr at RT and then with paraffin at 65 ℃ for 90 minutes twice, and then embedded in paraffin. The lungs were sectioned at 8 μm on a microtome.

For histologic analysis of organoid assays, transwells were fixed in 4% PFA overnight at 4 ℃, then washed in PBS overnight at least three times. Transwells were cut and embedded in OCT, then 8 μm sections were cut on a cryostat.

For immunofluorescent staining, paraffin sections were incubated in xylene for 10 minutes twice, then rehydrated in ethanol washes (100% twice, 95%, 70%, 50% ethanol) for 5 minutes each. OCT embedded slides were fixed in 4% PFA at RT for 10 minutes, then washed three times with PBS. For both paraffin and OCT embedded slides, antigen retrieval (Cat#DV2004MX; Biocare Medical; Cat#322000; Advanced Cell Diagnostics) was performed for 30 minutes at 95 ℃. Slides were washed with 0.1% Tween 20 in PBS (PBST) 3 times for 5 minutes. Slides were then incubated in blocking buffer (3% donkey serum in PBST) for at least 1 hour, then incubated overnight in primary antibodies in 1% donkey serum in PBST at 4 ℃. The following primary antibodies were used for mouse tissue: chicken anti-GFP (Cat#GFP-1020; Aves Labs; used 1:250), goat anti-GFP (Cat#ab6673, Abcam; used 1:250), rabbit anti-SMA (Cat#ab5694; Abcam; used 1:200), rabbit anti-DES (Cat#ab15200; Abcam; used 1:200), goat anti-SCGB1a1 (Cat#sc-9772; Santa Cruz; used 1:500), mouse anti-SCGB1a1 (Cat#sc-390313; Santa Cruz; used 1:200), rabbit anti-SFTPC (Cat#AB3786; Millipore Sigma; used 1:2000), goat anti-SFTPC (Cat#sc-7706; Santa Cruz; used at 1:200), chicken anti-KRT5 (Cat#905901; BioLegend; used at 1:500), goat anti-SOX2 (Cat#GT15098; Neuromics; used 1:200), rat anti-RAGE (Cat#MAB1179; R&D Systems; used at 1:200), chicken anti-RFP (Cat#600–901-379S; Rockland; used 1:200), rabbit anti-RFP (Cat#600–401-379; Rockland; used 1:100), mouse anti-TubIV (Cat#ab11315; Abcam; used 1:200), rabbit anti-p63 (Cat#13109T; Cell Signaling Technology; used 1:200), rabbit anti-NGFR (Cat#ab8875; Abcam; used 1:200), mouse anti-KRT14 (Cat#CBL197; Sigma; used 1:100), and rabbit anti-p-SMAD1/5/8 (Cat#AB3848-I; Millipore Sigma; used 1:100).

The following primary antibodies were used for human tissue: rabbit anti-SMA (Cat#ab5694; Abcam; used 1:200), rabbit anti-p-SMAD1/5/8 (Cat#AB3848-I; Millipore Sigma; used 1:100), chicken anti-KRT5 (Cat#905901; BioLegend; used at 1:500), goat anti-SOX2 (Cat#GT15098; Neuromics; used 1:200), goat anti-SFTPC (Cat#sc-7705; Santa Cruz; used at 1:200), rabbit anti-p63 (Cat#13109T; Cell Signaling Technology; used 1:200), rabbit anti-NGFR (Cat#ab8875; Abcam; used 1:200), and mouse anti-KRT14 (Cat#CBL197; Sigma; used 1:100). Slides were washed with PBST and then incubated for 1 hour at RT in secondary antibodies diluted in PBST. The following secondary antibodies were used at 1:250: Donkey anti-Chicken IgG (H+L) Alexa Flour 488 (Cat#703–545-155; Jackson ImmunoResearch), Donkey anti-Rabbit IgG Alexa Flour 555 (Cat# A-31572; Thermo Fisher), Donkey anti-Goat Alexa Flour 647 (Cat# A-21447; Thermo Fisher), Donkey anti-Rat DyLight 488 (Cat#SA5–10026; Thermo Fisher), and Donkey anti-Mouse IgG Alexa Flour 555 (Cat# A-31570; Thermo Fisher). DAPI (0.2 μg/mL) (Cat#1738176; Thermo Fisher) was added for 5 minutes, and slides were then mounted with TrueBlack to reduce background and Fluorosave to maintain fluorescence.

Lung digestion and Fluorescence Activated Cell Sorting (FACS)

For mouse, whole lung was dissected from adult animals and tracheally perfused with a digestion cocktail of Collagenase Type I (Cat#17100017; Thermo Fisher; used 225 U/mL), Dispase II (Cat#17105041; Thermo fisher; used 15 U/mL) and Dnase I (Cat#DN25; Sigma-Aldrich; used 50 U/mL) and removed from the chest. The lung was further diced with a razor blade and incubated in digestion cocktail for 45 mins at 37 ℃ with continuous shaking. The mixture was then washed with sorting buffer (2% FBS and 1% Penicillin-Streptomycin in DMEM (Cat#31053028; Thermo Fisher)). The mixture was passed through a 70 μm cell strainer and resuspended in RBC lysis buffer (Cat#NC9067514; Thermo Fisher), then passed through a 40 μm cell strainer. Cell suspensions were incubated with the appropriate conjugated antibodies in sorting buffer for 30 min at 4 ℃ and washed with sorting buffer. FACS sorting was performed on a BD FACSAria II using FACSDiva software. Doublets and dead cells were excluded based on forward and side scatter and DRAQ7 (Cat#7406S; Cell Signaling Technologies) fluorescence, respectively. Immune and endothelial cells were excluded using CD45 (Alexa Flour 700; Cat#560510; BD; used 1:200; clone 30-F11) and CD31 (APC/Fire750; Cat#102528; BioLegend; used 1:200; clone MEC13.3), respectively. For $Gli1^{EGFP}$ and $Gli1^{creERT2/+}:R26^{YFP/YFP}$ sorting, epithelial cells were also excluded using CD326 (BV421; Cat#563214; BD; used 1:200; clone G8.8), then $Gli1$ cells were sorted using endogenous GFP fluorescence. For ITGB4 sorting, cells were selected for CD326 and then CD104 (PE; Cat#123610; BioLegend; used 1:100 or Alexa Flour 647; Cat#123608; BioLegend; used 1:75; clone 346–11A). Cells were sorted into sorting buffer. Analysis was performed using FlowJo v10 software.

For human, multiple pieces were collected from whole lungs and separated into smaller pieces for a total of approximately 1 gram. Tissue was cut with scissors and resuspended in a digestion cocktail of 0.25% Collagenase A (Cat#SCR136; Millipore Sigma), Dispase II (Cat#17105041; Thermo fisher; used 15 U/mL) and Dnase I (Cat#DN25; Sigma-Aldrich; used 50 U/mL) in RPMI (Cat#R7388; Millipore Sigma). The tissue was digested at 37 ℃ for 1 hour with intermittent resuspension. Cells were passed through a 100 μm cell strainer,

washed with PBS, and resuspended in 0.5% BSA in PBS. Single cells were selected and mesenchymal cells were sorted using the following gating strategy: DAPI-, CD31- (PE/Cy7; Cat#303118; BioLegend; used 1:200; clone WM59), CD45- (APC; Cat#304037; BioLegend; used 1:200; clone HI30), CD326- (FITC; Cat#324204; BioLegend; used 1:200; clone 9C4), and CD235a- (APC/Cy7; Cat#349116; BioLegend; used 1:200; clone HI264).

Single Cell Capture and Sequencing

For mouse scRNA-seq, all live *Gli1* Lin+ cells were sorted from two *Gli1*$^{creERT/+}$:$R26$$^{YFP/YFP}$ adult lungs. *Gli1* Lin+ cells were isolated based on forward and side scatter, DAPI exclusion, and GFP fluorescence. One mouse was challenged with repetitive bleomycin and one was treated with PBS at the same timepoints as a control. The sorted *Gli1* Lin+ cells from each animal were separately resuspended in 50 μL PBS with 0.04% BSA at 1,000 cells/μL. For human scRNA-seq, sorted (live, CD31-, CD45-, CD326-, CD235a-) healthy and IPF mesenchymal cells were resuspended in 0.05% BSA in PBS. Cells were loaded onto a single lane per sample into the Chromium™ Controller to produce gel bead-in emulsions (GEMs). GEMs underwent reverse transcription for RNA barcoding and cDNA amplification, with the library prepped using the Chromium Single Cell 3' Reagent Version 2 kit. Each sample was sequenced in 1 lane of the HiSeq2500 (Illumina) in Rapid Run Mode.

Cell Culture

For *Ubc*$^{creERT2/+}$:$R26$$^{SmoM2/+}$ mesenchymal cells, lung was digested as above and then cultured on gelatin-treated tissue culture plates in DMEM/F-12 (Cat#11330032; Thermo Fisher) with 10% FBS and 1% Penicillin-Streptomycin. Media was refreshed every other day and primary lung mesenchymal cells were maintained for no more than five passages. The *Ubc*$^{creERT2/+}$:$R26$$^{SmoM2/+}$ mesenchymal cells were treated with vehicle or 1 μg/ml 4-OH-tamoxifen (4OHT) (Cat#579002; Millipore Sigma) for 72 hrs. When used for organoid assays, 4OHT treatment occurred for 72 hours immediately prior to co-culture with epithelium. Where applicable, cells were treated with vehicle or 4 ng/mL TGF-β1 (Cat#100–21; PeproTech) for 72 hours.

Organoid Assay

Adult mouse lungs were FACS sorted for ITGB4+ epithelial progenitor cells and *Gli1*+ or *Gli1* Lin+ mesenchymal cells. The trachea was dissected and removed from the lung prior to lung digestion and FACS sorting. ITGB4+ epithelial cells and *Gli1* mesenchymal cells were co-cultured (1.5x10^4 epithelial cells : 5x10^4 mesenchymal cells/well) in a modified MTEC media diluted 1:1 in growth factor reduced matrigel (Cat#CB-40230A; Thermo Fisher). Modified MTEC culture media (Cat#CC-3118; Lonza) is comprised of small airway basal media (SABM) with selected components from SAGM bullet kit including Insulin, Transferrin, Bovine Pituitary Extract, Retinoic Acid, and human Epidermal Growth Factor. 0.1 μg/mL cholera toxin (Cat#C8052; Sigma Aldrich), 5% FBS, and 1% Penicillin-Streptomycin were also added to the media. Cell suspension-matrigel mixture was placed in a transwell and incubated in growth media with 10 μM ROCK inhibitor (Cat#72252; STEMCELL Technologies) in a 24 well plate for 48 hours, after which the media was replenished every other day (lacking ROCK inhibitor). Each experimental condition was

performed in triplicates. Where applicable, recombinant BMP4 (Cat#314-BP-010; R&D Systems; used 50 ng/mL) and GREM2 (Cat#2069-PR-050; R&D Systems; used 1.5 μg/mL) were added to the media after 48 hours and replenished in every media change. Colonies were assayed after 12–14 days.

To extract RNA from the organoid assays, cell suspension-matrigel mixtures in the transwells were washed with PBS and incubated in a digestion cocktail of Collagenase Type I (Cat#17100017; Thermo Fisher; used 225 U/mL), Dispase II (Cat#17105041; Thermo fisher; used 15 U/mL) and Dnase I (Cat#DN25; Sigma-Aldrich; used 50 U/mL) for 1 hour at 37 ºC with intermittent resuspension. The mixture was removed from the transwell and resuspended in TrypLE (Cat#12563011; Thermo Fisher) and shaken at 37 ºC for 20 minutes. Cells were resuspended in sorting buffer (2% FBS and 1% Penicillin-Streptomycin in DMEM) and blocked with rat serum (Cat#19860; STEMCELL Technologies; used 1:50) for 10 minutes at 4 ºC. Cells were then stained with biotin anti-mouse CD326 (Cat#118204; BioLegend; clone G8.8; used 1:250) for 30 minutes at 4 ºC. Streptavidin beads (Cat#19860; STEMCELL Technologies; used 1:50) were added to isolate the epithelial cells.

Quantitative RT-PCR

Total RNA was obtained from cells isolated from organoid assays or cultured primary lung fibroblasts using the PicoPure RNA Isolation Kit (Cat#KIT0204; Applied Biosystems) or the RNeasy Kit (Cat#74004; QIAGEN), following the manufacturers' protocols. RNA from mouse lung tissue was obtained by removing the entire left lobe, homogenizing in trizol (Cat#15596018; Thermo Fisher), and extracting RNA using the E.Z.N.A Total RNA Kit (Cat#R6834–01; Omega Bio-Tek) following manufacturer instructions. cDNA was synthesized from total RNA using the SuperScript Strand Synthesis System (Cat#18080044, Cat#100000840; Thermo Fisher). Quantitative PCR was performed using the SYBR Green system (Cat#F415L; Thermo Fisher). Primers are listed in Supplementary Table 1. Relative gene expression levels after qRT-PCR were defined using the ΔΔCt method and normalizing to GAPDH.

RNAscope *In Situ* Hybridization

Paraffin-embedded lung sections were processed for RNA *in situ* detection of *Fbln2* (Cat#447931; Advanced Cell Diagnostics), *Npnt* (Cat#316771; Advanced Cell Diagnostics), and *Shh* (Cat#600951; Advanced Cell Diagnostics) using the RNAscope Multiplex Fluorescent Reagent Kit v2 (Cat#323100; Advanced Cell Diagnostics) according to the manufacturer's instructions.

Pulse Oximetry

The MouseOx Pulse Oximeter system (STARR Life Sciences) was used to measure arterial oxygen saturation from awake mice on the day of sacrifice. Mice were shaven prior to measurement. Mice were measured at 5 measurements per second for at least 5 minutes and at least 10 successful readings. All successful measurements (error code = 0) were averaged for each mouse.

Immunofluorescence Image Quantification

Sections were imaged for quantification on a Zeiss Lumar V12 microscope. At least three samples per genotype/condition were used, and at least 4 randomly selected regions were analyzed for each sample. Cell counts for SFTPC cells were performed on Fiji using the "Cell Counter" plug-in. Five high magnification images of randomly selected alveolar regions were counted per sample. SFTPC quantification is presented as a percentage of total DAPI+ cells as previously described[15]. Cell counts for DAPI were performed automatically by Fiji software using the "Analyze Particles" tool. Four low magnification images of randomly selected areas were analyzed per sample. Similar anatomic locations were taken for each sample. KRT5 area was calculated automatically in Fiji, and the units presented for KRT5 quantification are μm^2. For quantification by area, the image was first converted to 8 bit and the "Measure" function was used with a consistent threshold set to a minimum of 20 μm^2 and maximum of infinity. pSMAD1/5/8 quantification was similarly quantified by area and presented as a percentage of DAPI+ cells. Distance quantification was performed using Imaris 8.3.1 software. Surfaces were created for each marker of interest, and distance between two surfaces was calculated using the "Big Sortomato" tool in Imaris. Every distance measurement is presented as an individual datapoint, and the units of measurement are μm. For immunofluorescent quantification of organoids, all individual organoids from at least four non-consecutive sections (four Z positions of 3D culture) of each well were analyzed. Each organoid was classified based on expression of KRT5 and SFTPC. For each well, the number of KRT5+ and SFTPC+ organoids were expressed as a percentage of total organoids analyzed. For all analyses, performer was blinded to the specimen genotype/ condition during data collection and analysis. Results were averaged between each specimen and standard deviations were calculated per genotype/condition.

Single Cell RNA-Seq Analysis

To build transcript profiles of individual cells the CellRanger version 2.1.1 software with default settings was used for de-multiplexing, aligning reads with STAR software to GRCm38 for mouse genome and Hg19 for human, and counting unique molecular identifiers (UMIs). We used the Seurat R package along with a gene-barcode matrix provided by CellRanger for downstream analysis[36]. In total, we filtered the data in 2 different steps. We first filtered the dataset by only accepting cells that expressed a minimum of 200 genes and genes that were expressed in at least 3 cells. Our second filter was set to accept cells with less than 6000 unique gene counts and 5% mitochondrial counts. After removing unwanted cells, we used "LogNormalize" to normalize the gene expression measurements for each cell. We calculated 2,000 features that exhibit high cell-to-cell variation, which were used in principle component analysis (PCA) after scaling the data. We used the JackStrawPlot function in the Seurat package to create Scree plots and compare p-value (significance) for each principle component. We selected 10 different PCA's for clustering of both mouse and human cells. Clustering results were visualized using the Uniform Manifold Approximation and Projection (UMAP) algorithm in the Seurat package. For mouse datasets, we further integrated the PDGFRA+ clusters from both PBS and bleo samples to compare the datasets[37]. Differentially expressed genes between PBS and bleo datasets were identified using a MAST test in the DEseq package in R[38]. RNA velocity was calculated on the integrated object using Velocyto package and RNA velocity in

SeuratWrappers package in R^{21}. For human scRNA-seq analysis, we similarly integrated the PDGFRA+ clusters from both 3 healthy controls and 3 patients with IPF, and the differentially expressed genes were identified with a MAST test. For cluster visualization and individual gene visualization on all clusters we used the UMAP function. Gene ontology enrichment analysis was performed using the PANTHER Overrepresentation test[36] and entering the top differentially expressed genes with adj. p <0.1 and logfc >0.15 or <−0.15.

Statistics and Reproducibility

All statistical analyses were performed in GraphPad Prism 6.0 using unpaired one-tailed Student's t-tests to determine the P-value. Specific P values are labeled in the plots or figure legends, where significant values are P < 0.05. Ordinary one-way ANOVA was used for multiple comparison to a control group. All data in graphs are presented as mean ± SD. No data was excluded from the analyses presented in this study. All animal studies were independently performed twice with successful replication, except for the single cell RNA-sequencing. All *in vitro* experiments were performed at least three times with successful replication. Three or more biological replicates were used for every study and specific n values are listed in the figure legends.

Reporting Summary

Further information is available in the Reporting Summary.

Extended Data
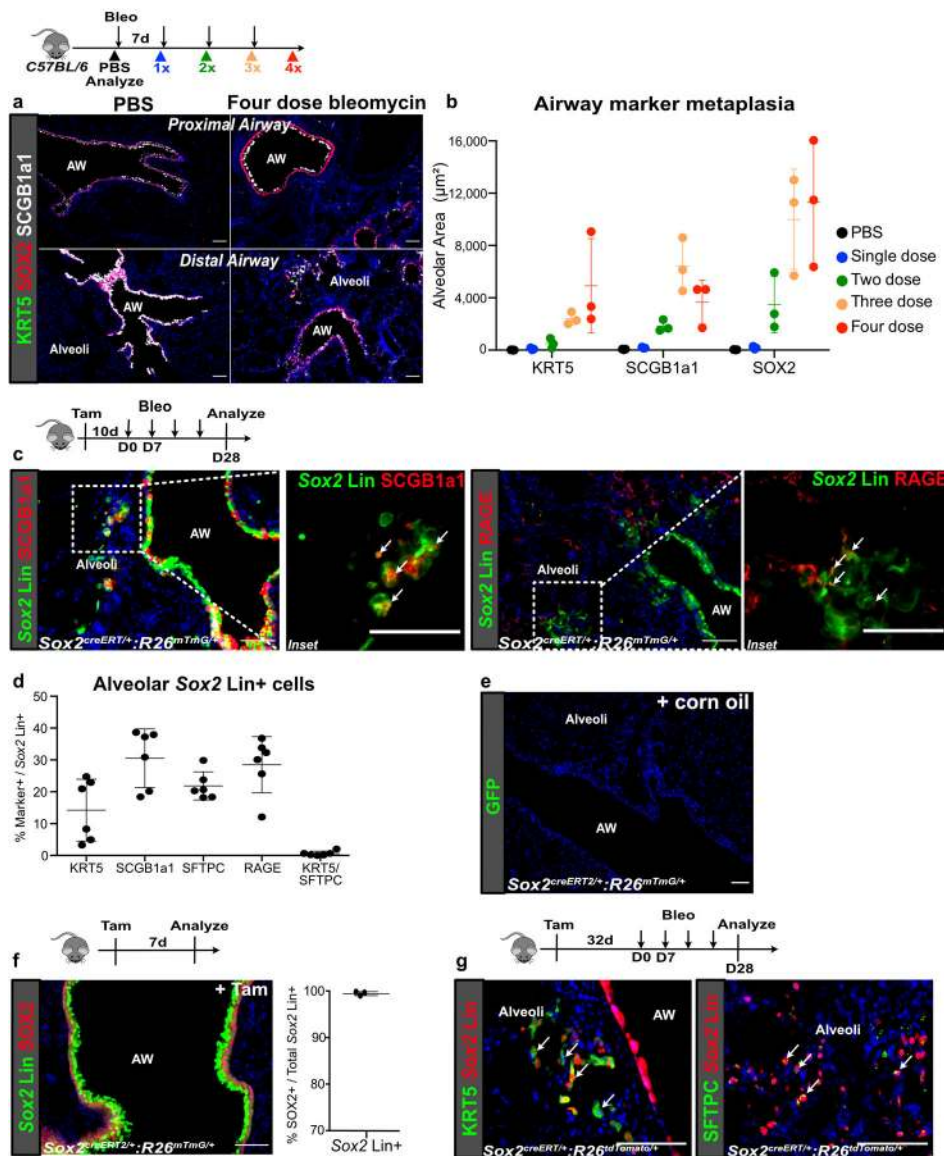
Extended Data Fig. 1. Epithelial progenitors expand distally in fibrotic repair

(**a,b**) Time course showing appearance of metaplastic airway epithelium in the alveoli after 1, 2, 3 or 4 doses of weekly bleomycin injury. (n = 3 per group; each data point represents one animal). Data are expressed as mean ± SD.

(**c,d**) Contribution of *Sox2* Lin+ cells to the various epithelial lineages in the alveoli after bleomycin injury. (n = 6 per group; each data point represents one animal; one-tailed unpaired Student's *t*-test). Data are expressed as mean ± SD.

(**e**) Lack of *Sox2* Lin+ cells in corn oil-treated *Sox*^{creERT2}:*R26*^{mTmG} lung. (2 animals)

(**f**) Co-localization of Sox2 Lin+ cells and SOX2 staining. (n = 3 animals). Data are expressed as mean ± SD.

(**g**) Extended washout after tamoxifen (>4wks) followed by bleomycin demonstrates similar expansion of *Sox2* Lin+ cells into the alveoli (3 animals).

AW = airway. Scale bars, 100 μm.
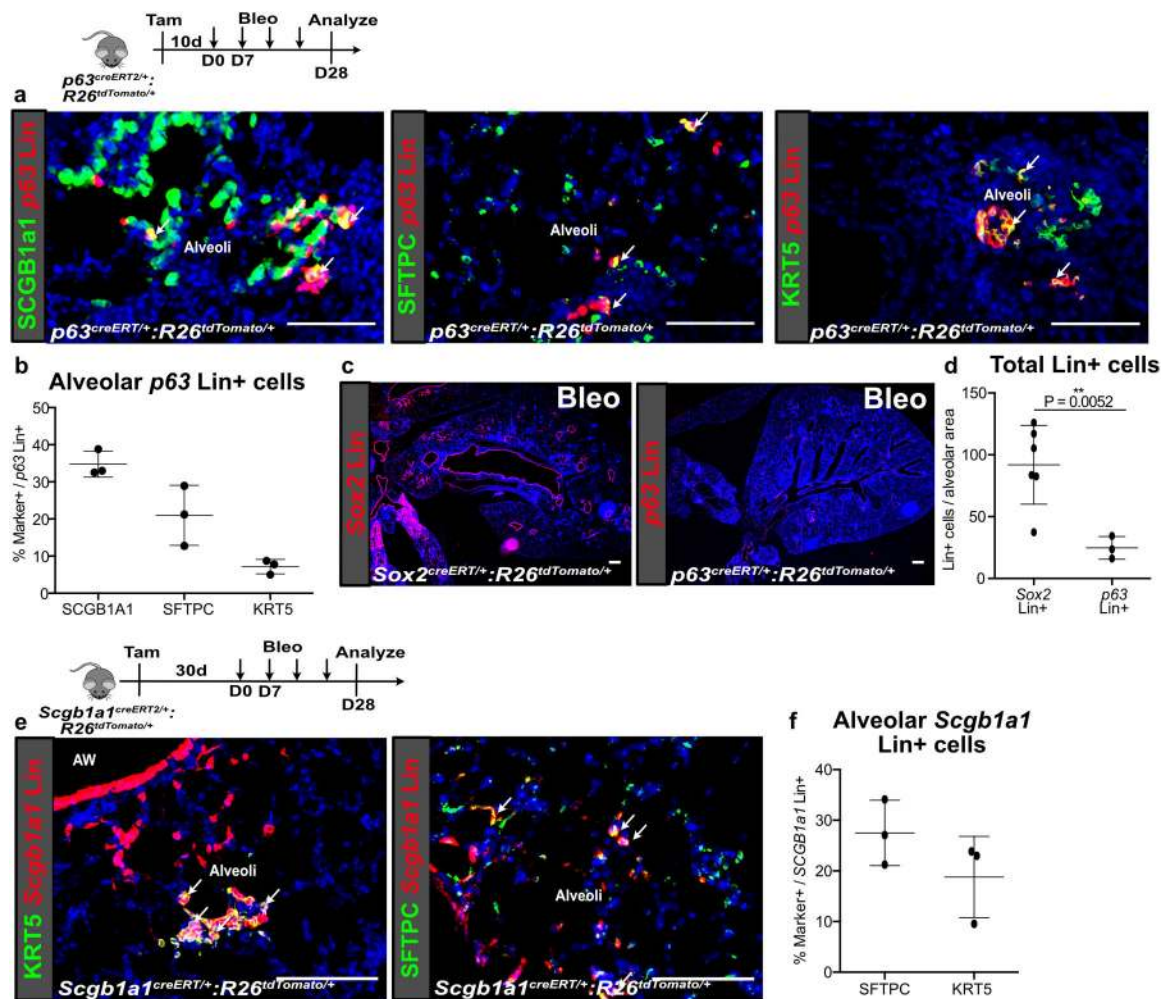
Extended Data Fig. 2. Lineage tracing of diverse airway progenitors after bleomycin injury

(**a,b**) *p63* Lin+ cells also expanded into the alveoli after bleomycin but did not contribute significantly to KRT5+ basal cells in the alveoli. (n = 3 animals). Data are expressed as mean ± SD.

(**c,d**) Comparison of *p63* Lin+ and *Sox2* Lin+ cells that expand into the alveoli after bleomycin injury. (n = 3 for *p63* Lin, n = 6 for *Sox2* Lin; each data point represents one animal; one-tailed unpaired Student's *t*-test). Data are expressed as mean ± SD.

(**e,f**) Contribution of *Scgb1a1* Lin+ cells to the various epithelial lineages in the alveoli after bleomycin injury. (n = 3 per group; each data point represents one animal). Data are expressed as mean ± SD.

AW = airway. Scale bars, 100 μm.
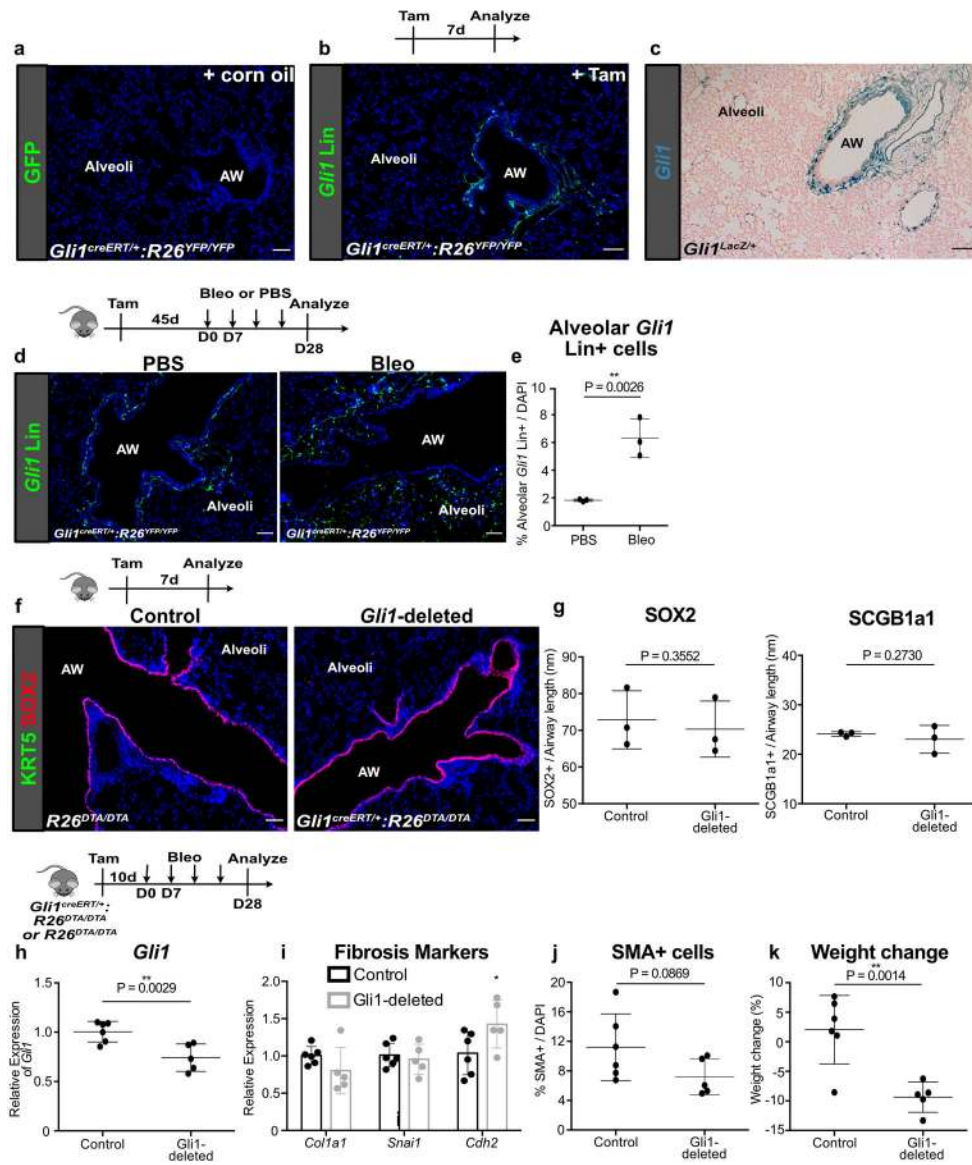
Extended Data Fig. 3. *Gli1* Lin+ mesenchyme expands distally in fibrotic repair
(**a**) Lack of *Gli1* Lin+ cells in corn oil-treated *Gli1^creERT2^:R26^YFP^* lung (2 animals).
(**b,c**) Comparison of *Gli1* Lin+ cell localization with *Gli1+* cells in *Gli1^LacZ/+^* lung. These experiments were each repeated three times independently with similar results.
(**d,e**) Extended washout after tamoxifen (>4wks) followed by bleomycin demonstrates similar expansion of *Gli1* Lin+ cells into the alveoli. (n = 3 per group; each data point represents one animal; one-tailed unpaired Student's *t*-test). Data are expressed as mean ± SD.
(**f,g**) Deletion of *Gli1+* cells does not alter airway epithelial composition during normal homeostasis. (n = 3 per group; each data point represents one animal; one-tailed unpaired Student's *t*-test). Data are expressed as mean ± SD.
(**h-j**) *Gli1*-deleted lungs treated with bleomycin demonstrate reduced expression of *Gli1* along with changes in fibrotic markers (n = 6 for control, n = 5 for Gli1-deleted; each data

point represents one animal; for (i), *Col1a1* P = 0.0862; *Snai1* P = 0.3126; *Cdh2* P = 0.0310; one-tailed unpaired Student's *t*-test for (h-j)). Data are expressed as mean ± SD.

(k) Weight loss after bleomycin injury in control and *Gli1*-deleted animals (n = 6 for control, n = 5 for Gli1-deleted; each data point represents one animal; one-tailed unpaired Student's *t*-test). Data are expressed as mean ± SD.

AW = airway. Scale bars, 100 μm.
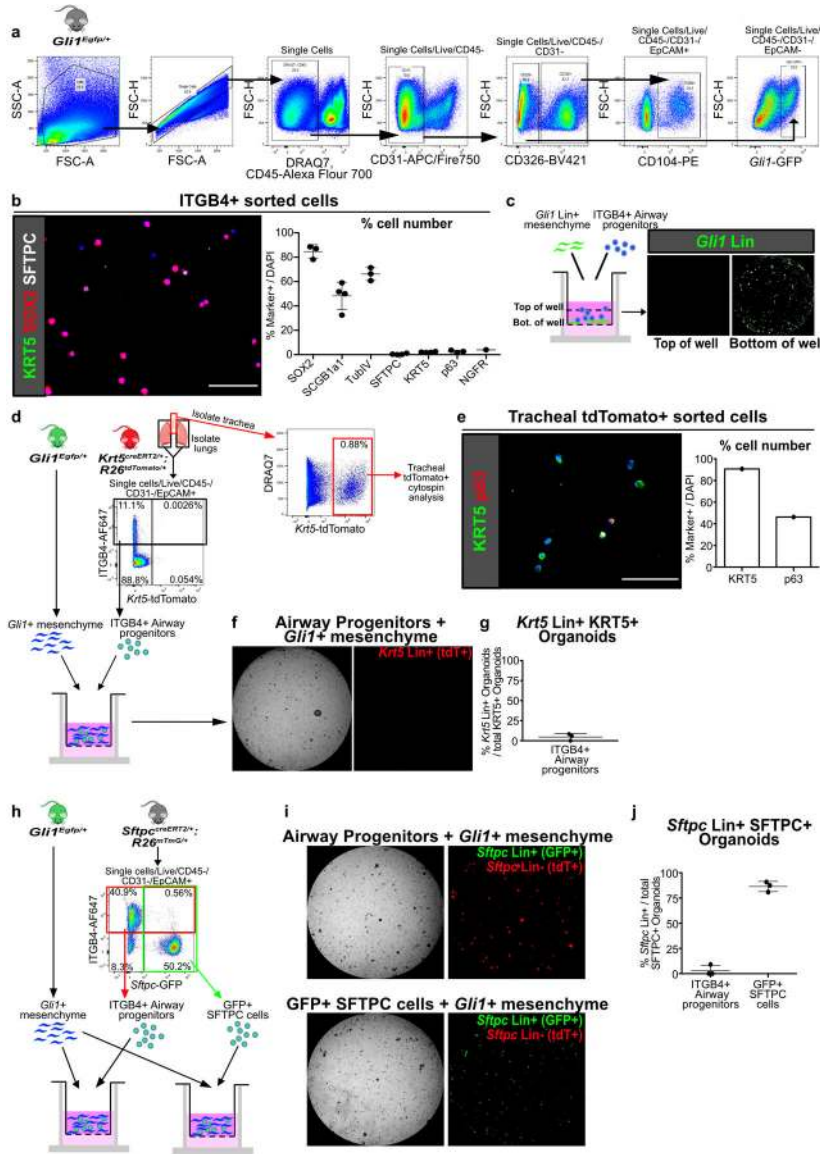
Extended Data Fig. 4. ITGB4+ airway progenitors give rise to KRT5+ and SFTPC+ cells that are not from pre-existing *Krt5*+ and *Sftpc*+ cells

(**a**) Gating strategy for isolation of ITGB4+ airway progenitors and *Gli1*+ mesenchymal cells by FACS, presented in figures 2a,e; 3f; 5e; 6f and extended data figures 4d,h; 5h; 8g.

(**b**) Cytospin of freshly sorted ITGB4+ confirms that majority of cells are SOX2+, SCGB1A1+, and TubIV+, with cells rarely positive for SFTPC, KRT5, p63, or NGFR (n = 1

for NGFR, n = 3 for rest; each data point represents one biological replicate). Data are expressed as mean ± SD.

(**c**) Z-axis scan shows that *Gli1* Lin+ mesenchyme settle to bottom of the Matrigel well.

(**d-g**) Lineage trace of pre-existing *Krt5* Lin+ (tdTomato+) cells followed by isolation of lung for ITGB4+ airway progenitor organoid culture with *Gli1*+ cells. Tracheal *Krt5* Lin+ cells demonstrate expression of basal cell markers KRT5 and p63 (**e**), while few *Krt5* Lin+ cells appear in ITGB4+ cell-derived organoid isolated from the lung of the same animal (**f,g**). The overwhelming majority of KRT5+ cells in the ITGB4-derived organoids are *Krt5* Lin-negative. (n = 3 wells for (f,g); n = 1 sample for (e)). Data are expressed as mean ± SD.

(**h-j**) Lineage trace of pre-existing *Sftpc* Lin+ (membrane GFP+) cells followed by isolation of the lung epithelium for organoid culture with *Gli1*+ cells. ITGB4+ (red box) or *Sftpc* Lin + (green box) cells were sorted from the same lung. The overwhelming majority of SFTPC+ organoids in the ITGB4-derived organoids are *Sftpc* Lin-negative, while most SFTPC+ cells in the *Sftpc* Lin+ derived organoids are Lin+ (n = 3; each data point represents one well). Data are expressed as mean ± SD. Scale bars, 100 μm.
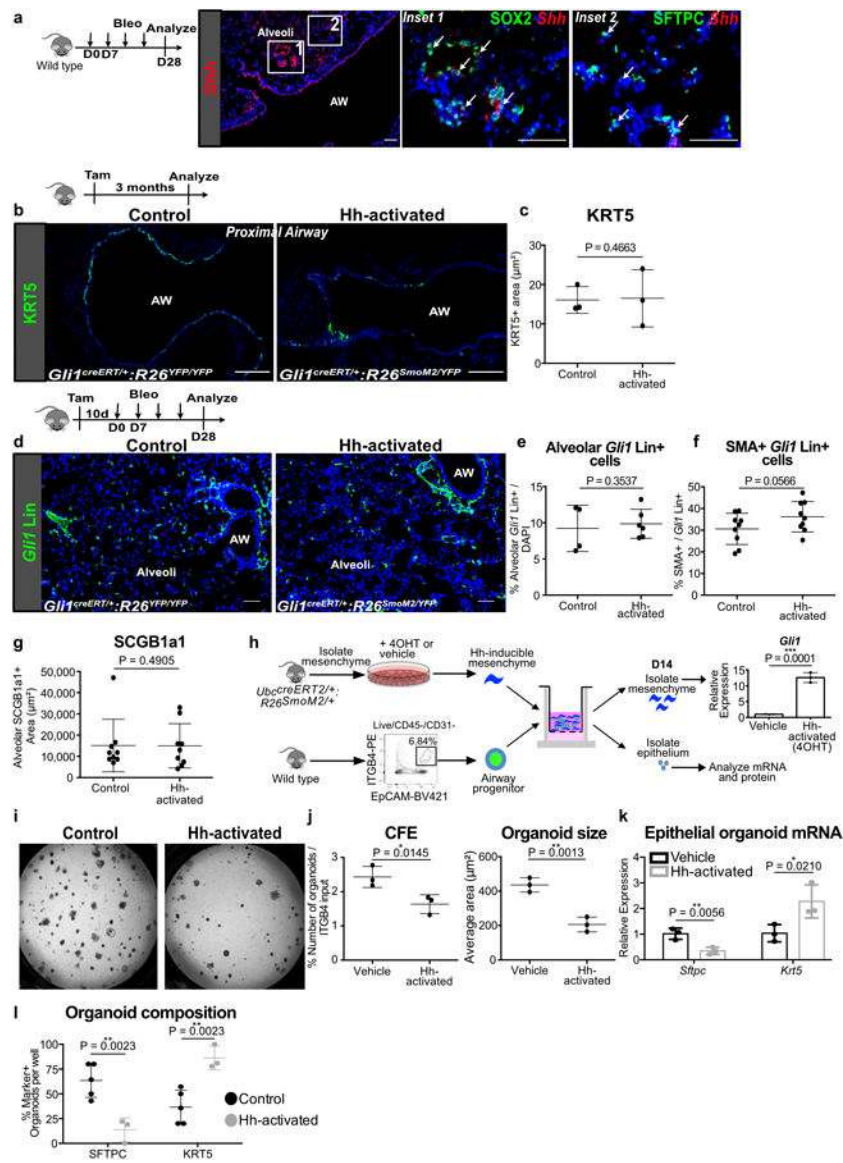
Extended Data Fig. 5. Characterization of Hh-activation during homeostasis and in fibrotic repair

(**a**) RNAScope *in situ* of *Shh* shows expression in ectopic SOX2+ cells in the alveoli after bleomycin injury. This experiment was repeated independently twice with similar results.

(**b,c**) Histology quantification shows no evidence of KRT5+ metaplasia in Hh-activated animals without injury when compared to controls (n = 3 per group; each data point represents one animal; one-tailed unpaired Student's *t*-test). Data are expressed as mean ± SD.

(**d-g**) After bleomycin injury, Hh-activated lungs show similar expansion of *Gli1+* cells in distal alveoli compared to controls, a trend towards increased myofibroblasts (SMA+) differentiation of the *Gli1* Lin+ cells in the alveoli, and no difference in ectopic SCGB1A1+ cells in the alveoli (for (e), n = 4 for control, n = 6 for Hh-activated; for (f,g), n = 9 per group; each data point represents one animal; one-tailed unpaired Student's *t*-test for (e-g)). Data are expressed as mean ± SD.

(**h**) Model of 3D airway organoid assay using Hh-inducible mesenchyme whereby pretreatment of 4-hydroxytamoxifen (4OHT) induces Hh activation in the mesenchyme as shown by upregulation of *Gli1* transcript compared to vehicle (ethanol) (n = 3 per group; each data point represents one biological replicate; one-tailed unpaired Student's *t*-test). (**i-l**) Mesenchymal Hh activation *in vitro* reduces CFE and organoid size, but increases the expression of *Krt5* and number of KRT5+ organoids while reducing *Sftpc* expression and number of SFTPC+ organoids ((i-k) n = 3 per group; (l) n = 3 for Hh-activated, n = 5 for control; each data point represents one well; one-tailed unpaired Student's *t*-test for (j-l)). Data are expressed as mean ± SD. Hh = hedgehog, 4OHT= 4-hydroxytamoxifen, AW = airway. Scale bars, 100 μm.
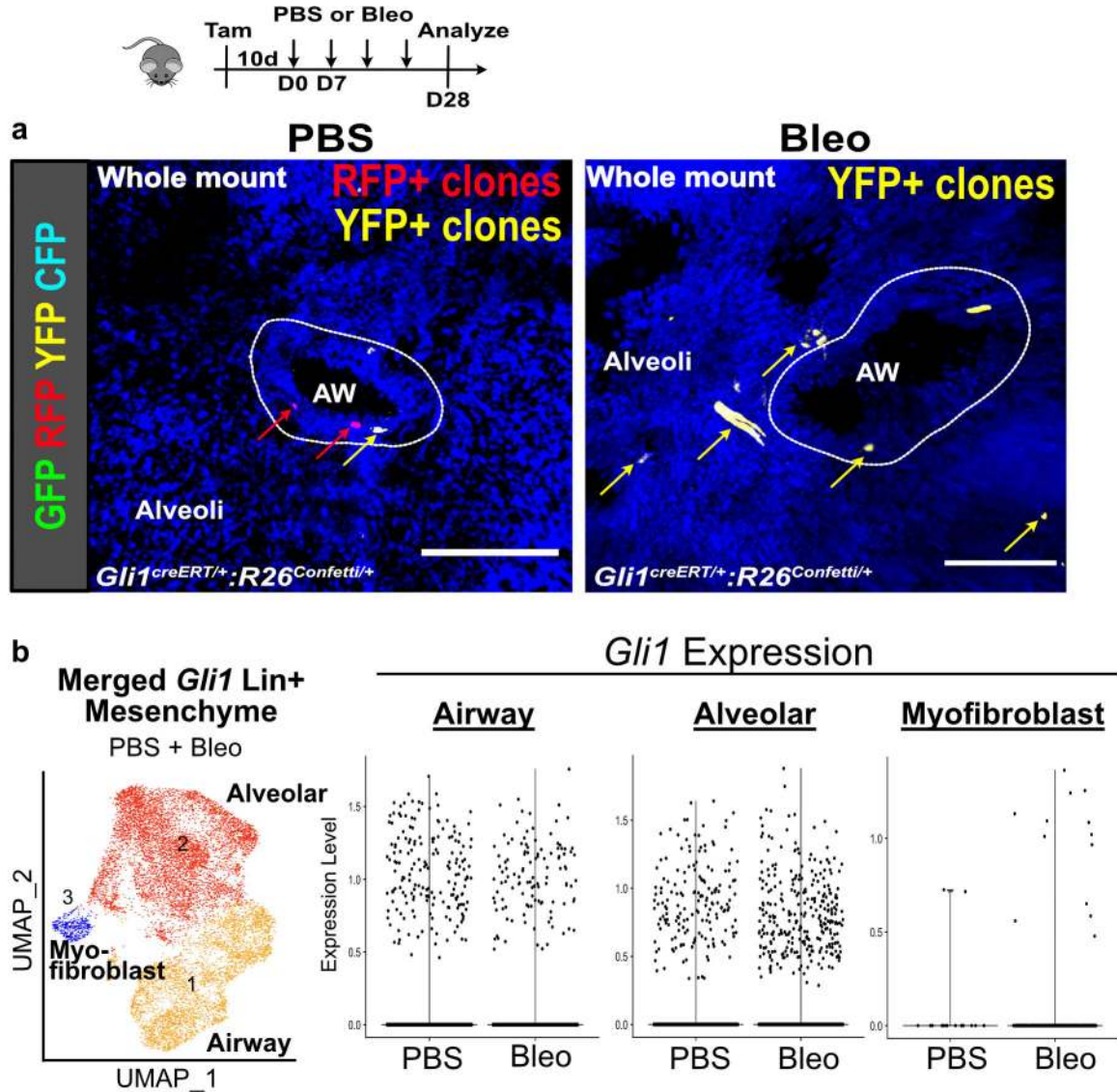
Extended Data Fig. 6. Expansion of *Gli1* Lin+ mesenchyme into the alveoli
(**a**) Multi-color stochastic recombination of *Gli1* Lin+ cells tagged with one of four possible fluorescent proteins (GFP, YFP, RFP, or CFP) shows clones of single color clustering around

the airway in PBS treated lungs, and clones of single color spanning the airway and alveoli following bleomycin injury (4 animals per group)

(b) Violin plots showing retention of *Gli1* expression in *Gli1* Lin+ cells following bleomycin injury as they migrate into the alveoli. Each black dot represents one cell (n values listed in source data for Figure 4d).

AW = airway. Scale bars, 100 μm.
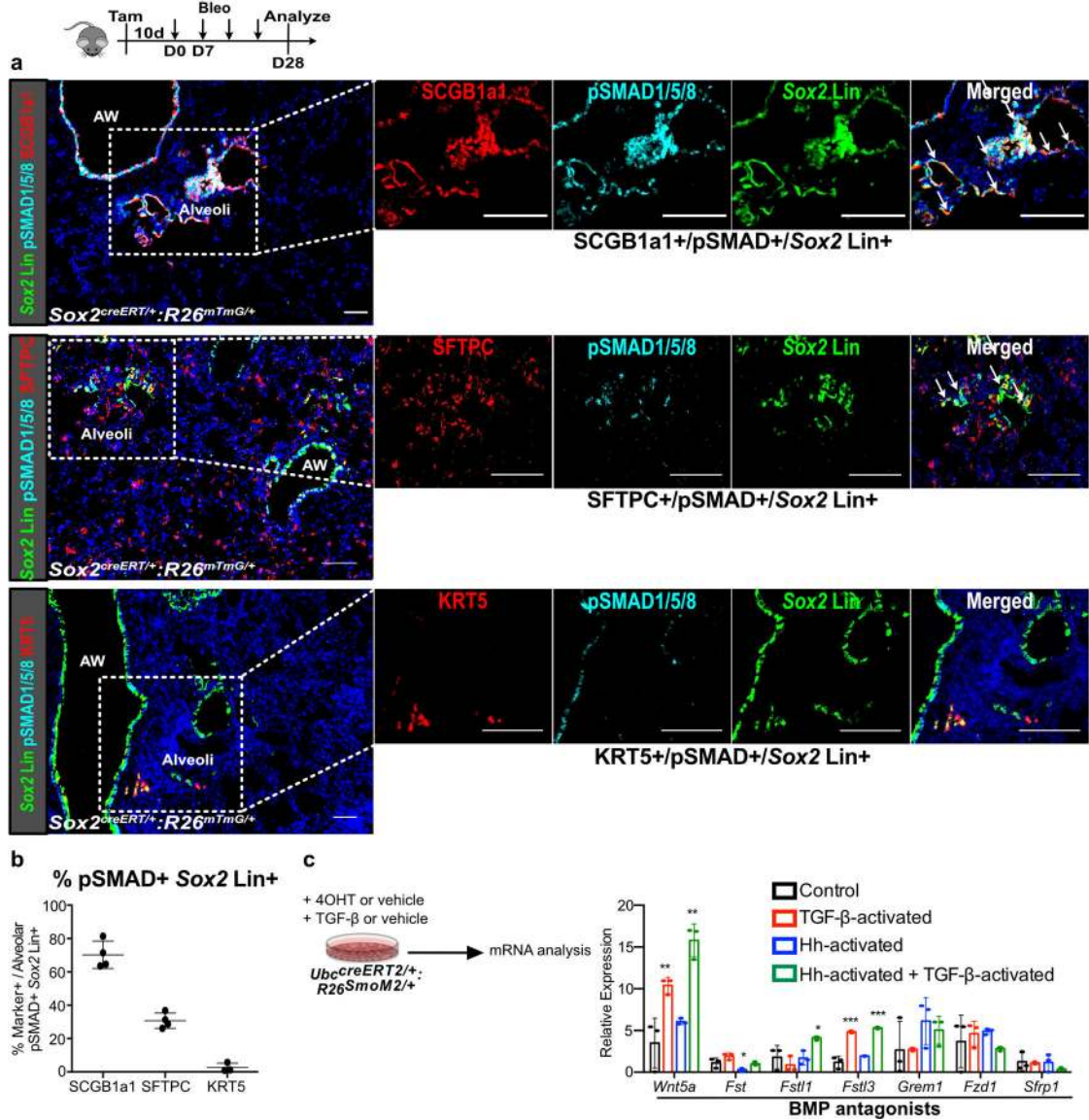
Extended Data Fig. 7. Spatial regulation of BMP activation

(**a,b**) pSMAD1/5/8 staining of *Sox2* Lin+ cells in the alveoli after bleomycin injury demonstrates that the majority of pSMAD1/5/8+/*Sox2* Lin+ cells are SCGB1A1+ or SFTPC +, and rarely KRT5+ (n = 3 for KRT5 quantification, n = 4 for SCGB1a1 and SFTPC quantification; each data point represents one animal). Data are expressed as mean ± SD.

(**c**) qPCR of Hh-inducible cultured mesenchyme isolated from $Ubc^{creERT2/+}:R26^{SmoM2/+}$ lungs treated with 4OHT +/- TGF-β, showing effect on various BMP antagonists expression (n = 3; each data point represents one biological replicate). *Wnt5a*: Control v TGF-β P = 0.0094, Control v Hh-activated P = 0.1066, Control v TGF-β + Hh-activated P = 0.002; *Fst*: Control v TGF-β P = 0.0598, Control v Hh-activated P = 0.0389, Control v TGF-β + Hh-activated P = 0.3833; *Fstl1*: Control v TGF-β P = 0.2051, Control v Hh-activated P = 0.4620, Control v TGF-β + Hh-activated P = 0.028; *Fstl3*: Control v TGF-β P = 0.0005, Control v Hh-activated P = 0.0704, Control v TGF-β + Hh-activated P = 0.0003; *Grem1*: Control v TGF-β P = 0.4845, Control v Hh-activated P = 0.2422, Control v TGF-β + Hh-activated P = 0.1417; *Fzd1*: Control v TGF-β P = 0.3341, Control v Hh-activated P = 0.2689, Control v TGF-β + Hh-activated P = 0.3320; *Sfrp1*: Control v TGF-β P = 0.4103, Control v Hh-activated P = 0.4614, Control v TGF-β + Hh-activated P = 0.1093; ordinary one-way ANOVA test. Data are expressed as mean ± SD. Scale bars, 100 μm.
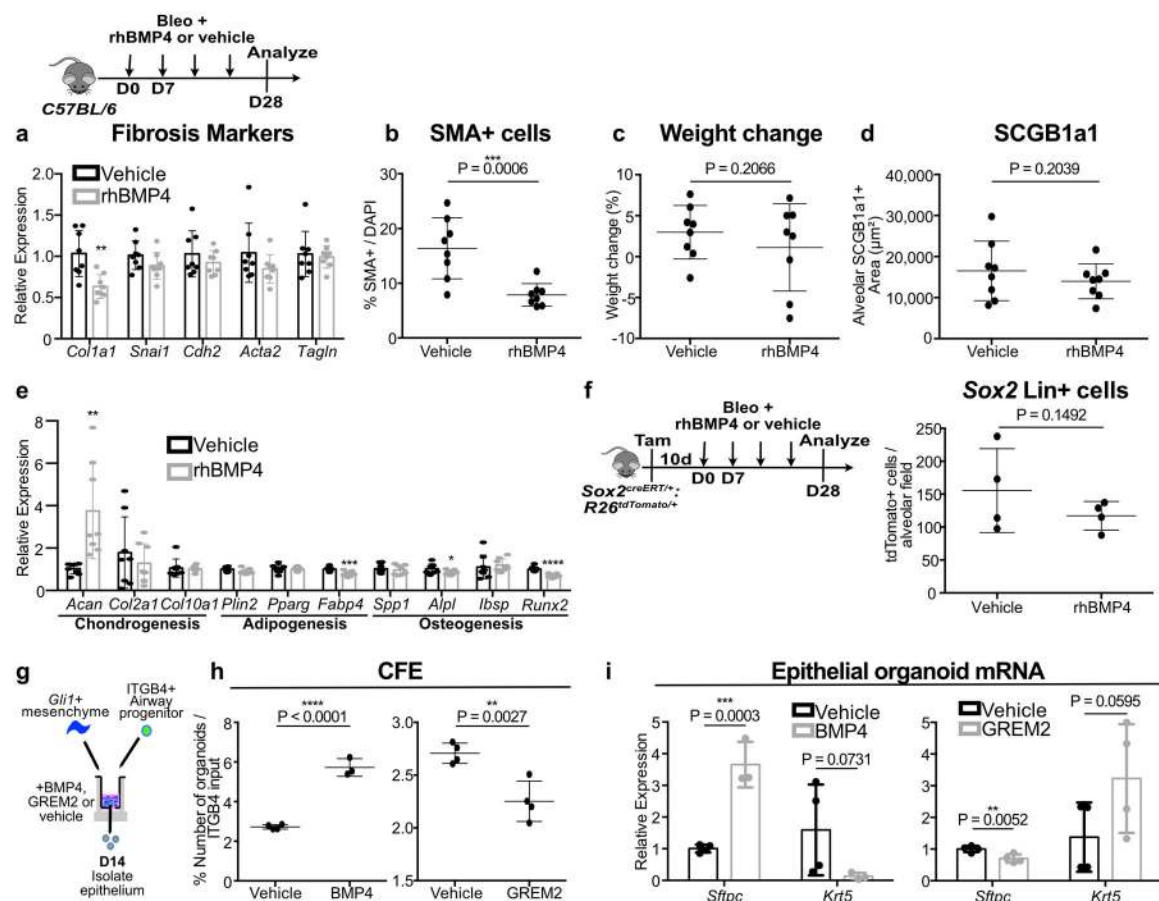
Extended Data Fig. 8. Effect of rhBMP4 *in vivo* and *in vitro*
(**a-d**) Effect of rhBMP4 treatment on fibrotic marker expression, myofibroblasts in the alveoli, weight change, and presence of ectopic SCGB1A1+ cells, in bleomycin injured C57BL/6 animals (n = 8 per group; each data point represents one animal). For (a), *Col1a1* P = 0.0015; *Snai1* P = 0.0769; *Cdh2* P = 0.1771; *Acta2* P = 0.0934; *Tagln* P = 0.3782.; one-tailed unpaired Student's *t*-test for (a-d). Data are expressed as mean ± SD.

(e) Effect of rhBMP4 on the expression of markers of chondrogenesis, adipogenesis, and osteogenesis in the lung (n = 8 per group; each data point represents one animal). *Acan* P = 0.0021; *Col2a1* P = 0.2363; *Col10a1* P = 0.4201; *Plin2* P = 0.0578; *Pparg* P = 0.4343; *Fabp4* P = 0.0006; *Spp1* P = 0.3117; *Alpl* P = 0.0474; *Ibsp* P = 0.3371; *Runx2* P < 0.0001; one-tailed unpaired Student's *t*-test. Data are expressed as mean ± SD.

(f) Effect of rhBMP4 on the total number of *Sox2* Lin+ cells in the alveoli after bleomycin injury (n = 4 per group; each data point represents one animal; one-tailed unpaired Student's *t*-test). Data are expressed as mean ± SD.

(g-i) Airway progenitor organoid co-cultured with *Gli1*+ mesenchyme treated with BMP4 demonstrates increased CFE and enhanced *Sftpc* expression with reduced *Krt5* (n = 4 for solvent, n = 3 for BMP4; each data point represents one well; one-tailed unpaired Student's *t*-test for (h,i)). Conversely, the BMP antagonist GREM2 acts to suppress CFE and *Sftpc* expression while enhancing *Krt5* (n = 4 per group; each datapoint represents one well; one-tailed unpaired Student's *t*-test for (h,i)). Data are expressed as mean ± SD.
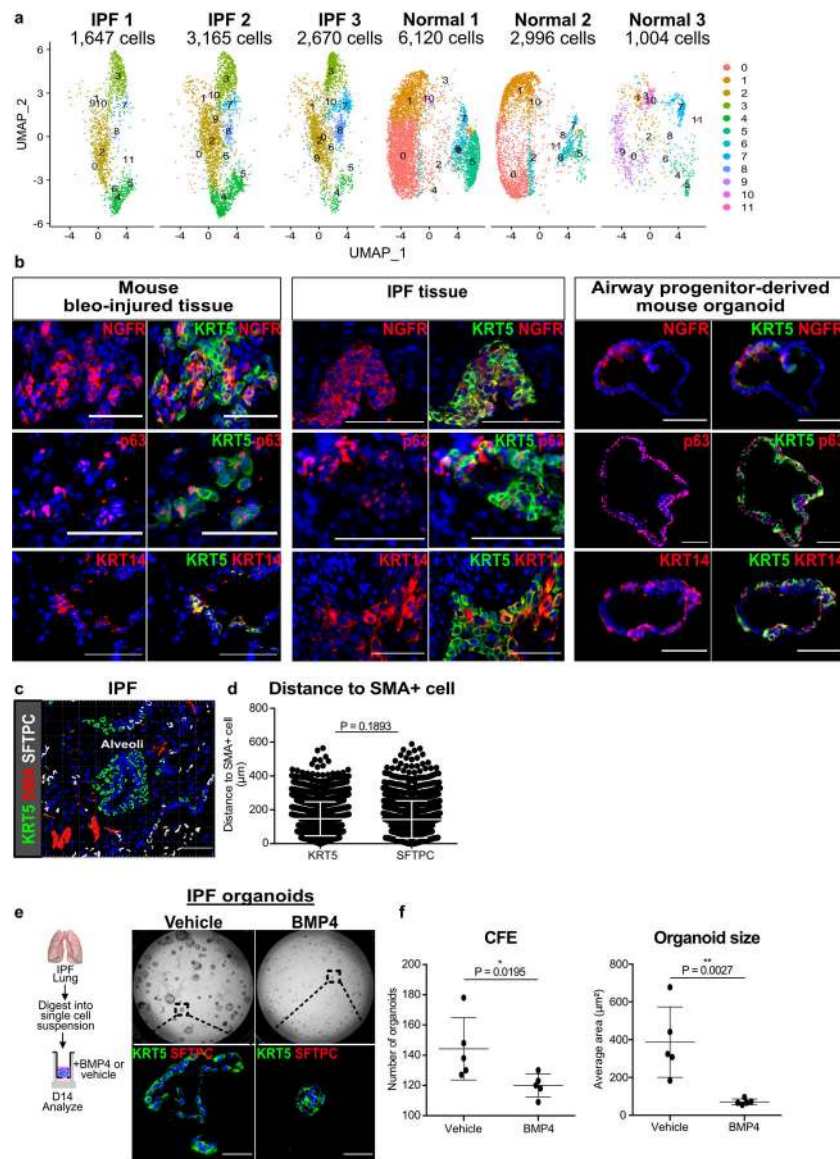
Extended Data Fig. 9. Metaplastic KRT5+ basal cells and SMA+ fibroblastic foci in the alveoli of IPF lungs

(a) UMAP projection of mesenchyme from each individual donor that was used in single cell RNA-seq analysis with contributing cell number.

(b) Expression of basal cell markers NGFR, p63, and KRT14, in KRT5+ basal cells in human IPF, along with mouse bleomycin injured lungs and murine airway progenitor-derived organoids. This experiment was repeated three times independently with similar results.

(c) Ectopic expression of KRT5 and SMA in the alveoli of IPF lungs form honeycomb cysts and fibroblast foci, respectively. This experiment was repeated independently twice with similar results.

(d) Average cell-to-cell distance shows equivalent proximity of metaplastic KRT5 and endogenous SFTPC cells to SMA+ fibroblastic foci (n = 3,280 KRT5 cells, n = 2,215

SFTPC cells; each datapoint represents an individual distance measurement with all measurements plotted for 3 samples; one-tailed unpaired Student's *t*-test).

(**e,f**) Unsorted epithelial organoids derived from dissociated IPF lungs grew KRT5+ organoids, and BMP4 attenuated the number and size of IPF-derived organoids. (n = 5; each data point represents one well; one-tailed unpaired Student's *t*-test) Data are expressed as mean ± SD. Scale bars, 100 μm.
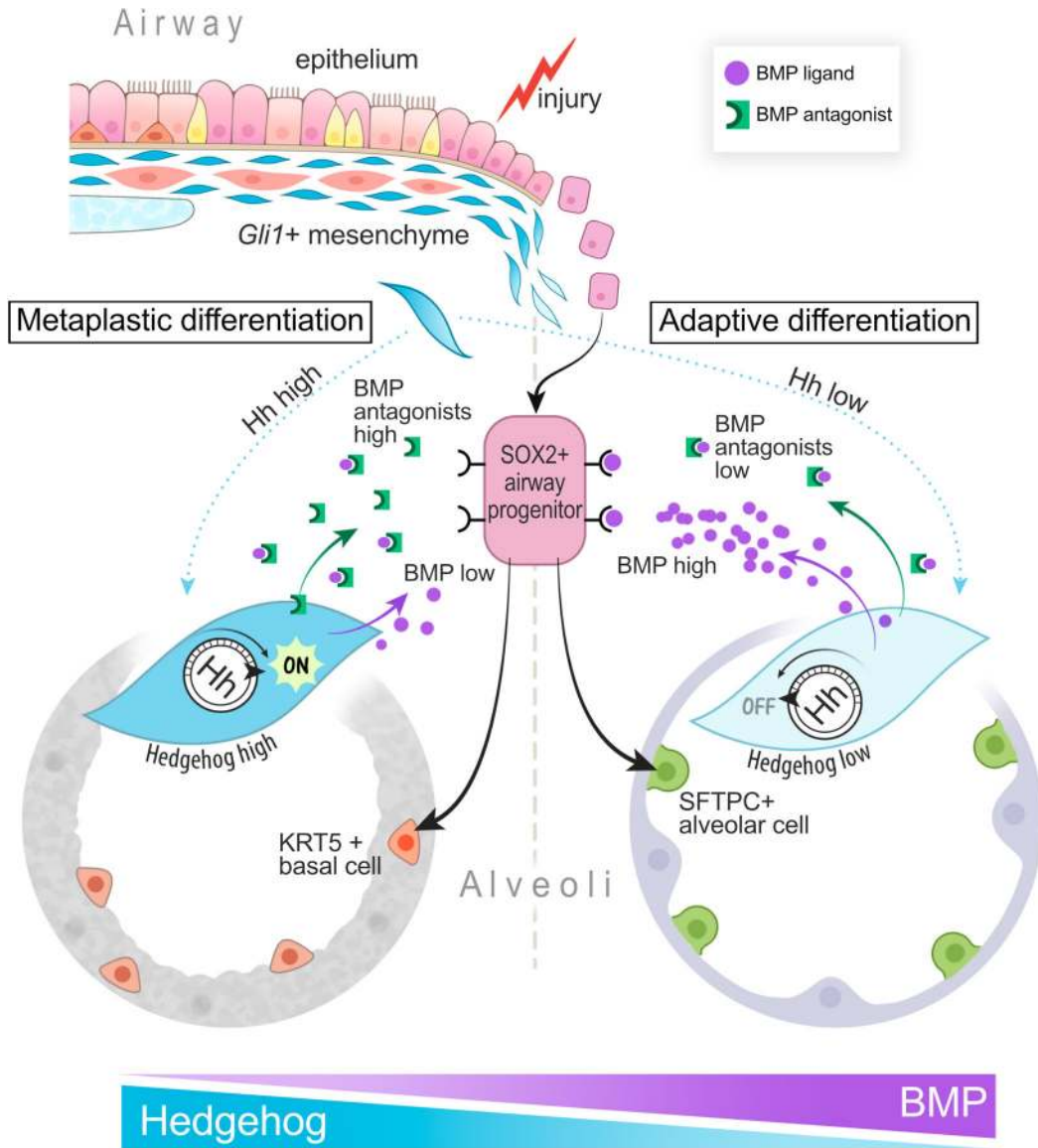
Extended Data Fig. 10. *Gli1*+ mesenchyme modulates SOX2+ progenitor fate
Model of *Gli1*+ mesenchyme integrating Hh activation as a rheostat that controls local BMP activation to determine SOX2+ airway epithelial progenitor fate.

Supplementary Material

Refer to Web version on PubMed Central for supplementary material.

Acknowledgements

Data Availability

The mouse RNA-seq data reported in this paper (Figure 4) is deposited in NCBI Gene Expression Omnibus (GEO) under the accession number GSE140032. The human RNA-seq data reported in this paper (Figure 7) is deposited in NCBI Gene Expression Omnibus (GEO) under the accession number GSE132771.

Previously published sequencing data from the Tabula muris cellular database was referenced here and is publicly available at https://tabula-muris.ds.czbiohub.org/.

There are no restrictions on data availability. All other data supporting the findings of this study are available from the corresponding author on reasonable request.

References

1. Giroux V & Rustgi AK Metaplasia: tissue injury adaptation and a precursor to the dysplasia-cancer sequence. Nat Rev Cancer 17, 594–604, doi:10.1038/nrc.2017.68 (2017). [PubMed: 28860646]

2. Chilosi M et al. Abnormal re-epithelialization and lung remodeling in idiopathic pulmonary fibrosis: the role of deltaN-p63. Lab Invest 82, 1335–1345 (2002). [PubMed: 12379768]

3. Seibold MA et al. The idiopathic pulmonary fibrosis honeycomb cyst contains a mucocilary pseudostratified epithelium. PLoS One 8, e58658, doi:10.1371/journal.pone.0058658 (2013). [PubMed: 23527003]

4. Xu Y et al. Single-cell RNA sequencing identifies diverse roles of epithelial cells in idiopathic pulmonary fibrosis. JCI Insight 1, e90558, doi:10.1172/jci.insight.90558 (2016). [PubMed: 27942595]

5. Prasse A et al. BAL Cell Gene Expression Is Indicative of Outcome and Airway Basal Cell Involvement in Idiopathic Pulmonary Fibrosis. Am J Respir Crit Care Med 199, 622–630, doi:10.1164/rccm.201712-2551OC (2019). [PubMed: 30141961]

6. Hogan BL et al. Repair and regeneration of the respiratory system: complexity, plasticity, and mechanisms of lung stem cell function. Cell Stem Cell 15, 123–138, doi:10.1016/j.stem.2014.07.012 (2014). [PubMed: 25105578]

7. Ray S et al. Rare SOX2(+) Airway Progenitor Cells Generate KRT5(+) Cells that Repopulate Damaged Alveolar Parenchyma following Influenza Virus Infection. Stem Cell Reports 7, 817–825, doi:10.1016/j.stemcr.2016.09.010 (2016). [PubMed: 27773701]

8. Vaughan AE et al. Lineage-negative progenitors mobilize to regenerate lung epithelium after major injury. Nature 517, 621–625, doi:10.1038/nature14112 (2015). [PubMed: 25533958]

9. Yang Y et al. Spatial-Temporal Lineage Restrictions of Embryonic p63(+) Progenitors Establish Distinct Stem Cell Pools in Adult Airways. Dev Cell 44, 752–761 e754, doi:10.1016/j.devcel.2018.03.001 (2018). [PubMed: 29587145]

10. Yee M et al. Alternative Progenitor Lineages Regenerate the Adult Lung Depleted of Alveolar Epithelial Type 2 Cells. Am J Respir Cell Mol Biol 56, 453–464, doi:10.1165/rcmb.2016-0150OC (2017). [PubMed: 27967234]

11. Peng T et al. Hedgehog actively maintains adult lung quiescence and regulates repair and regeneration. Nature 526, 578–582, doi:10.1038/nature14984 (2015). [PubMed: 26436454]

12. Zhao H et al. The suture provides a niche for mesenchymal stem cells of craniofacial bones. Nat Cell Biol 17, 386–396, doi:10.1038/ncb3139 (2015). [PubMed: 25799059]

13. Zhao H et al. Secretion of shh by a neurovascular bundle niche supports mesenchymal stem cell homeostasis in the adult mouse incisor. Cell Stem Cell 14, 160–173, doi:10.1016/j.stem.2013.12.013 (2014). [PubMed: 24506883]

14. Kramann R et al. Perivascular Gli1+ progenitors are key contributors to injury-induced organ fibrosis. Cell Stem Cell 16, 51–66, doi:10.1016/j.stem.2014.11.004 (2015). [PubMed: 25465115]

15. Wang C et al. Expansion of hedgehog disrupts mesenchymal identity and induces emphysema phenotype. J Clin Invest 128, 4343–4358, doi:10.1172/JCI99435 (2018). [PubMed: 29999500]

16. Xi Y et al. Local lung hypoxia determines epithelial fate decisions during alveolar regeneration. Nat Cell Biol 19, 904–914, doi:10.1038/ncb3580 (2017). [PubMed: 28737769]

17. Degryse AL et al. Repetitive intratracheal bleomycin models several features of idiopathic pulmonary fibrosis. Am J Physiol Lung Cell Mol Physiol 299, L442–452, doi:10.1152/ajplung.00026.2010 (2010). [PubMed: 20562227]

18. Kurche JS et al. Muc5b Enhances Murine Honeycomb-like Cyst Formation. Am J Respir Cell Mol Biol 61, 544–546, doi:10.1165/rcmb.2019-0138LE (2019). [PubMed: 31573335]

19. Jeong J, Mao J, Tenzen T, Kottmann AH & McMahon AP Hedgehog signaling in the neural crest cells regulates the patterning and growth of facial primordia. Genes Dev 18, 937–951, doi:10.1101/gad.1190304 (2004). [PubMed: 15107405]

20. Becht E et al. Dimensionality reduction for visualizing single-cell data using UMAP. Nat Biotechnol, doi:10.1038/nbt.4314 (2018).

21. La Manno G et al. RNA velocity of single cells. Nature 560, 494–498, doi:10.1038/s41586-018-0414-6 (2018). [PubMed: 30089906]

22. Tabula Muris C et al. Single-cell transcriptomics of 20 mouse organs creates a Tabula Muris. Nature 562, 367–372, doi:10.1038/s41586-018-0590-4 (2018). [PubMed: 30283141]

23. Zagorski M et al. Decoding of position in the developing neural tube from antiparallel morphogen gradients. Science 356, 1379–1383, doi:10.1126/science.aam5887 (2017). [PubMed: 28663499]

24. Massague J, Seoane J & Wotton D Smad transcription factors. Genes Dev 19, 2783–2810, doi:10.1101/gad.1350705 (2005). [PubMed: 16322555]

25. Plantier L et al. Ectopic respiratory epithelial cell differentiation in bronchiolised distal airspaces in idiopathic pulmonary fibrosis. Thorax 66, 651–657, doi:10.1136/thx.2010.151555 (2011). [PubMed: 21422041]

26. Tadokoro T, Gao X, Hong CC, Hotten D & Hogan BL BMP signaling and cellular dynamics during regeneration of airway epithelium from basal progenitors. Development 143, 764–773, doi:10.1242/dev.126656 (2016). [PubMed: 26811382]

27. Mou H et al. Dual SMAD Signaling Inhibition Enables Long-Term Expansion of Diverse Epithelial Basal Cells. Cell Stem Cell 19, 217–231, doi:10.1016/j.stem.2016.05.012 (2016). [PubMed: 27320041]

28. Bolanos AL et al. Role of Sonic Hedgehog in idiopathic pulmonary fibrosis. Am J Physiol Lung Cell Mol Physiol 303, L978–990, doi:10.1152/ajplung.00184.2012 (2012). [PubMed: 23023967]

29. Jia G et al. CXCL14 is a candidate biomarker for Hedgehog signalling in idiopathic pulmonary fibrosis. Thorax 72, 780–787, doi:10.1136/thoraxjnl-2015-207682 (2017). [PubMed: 28250200]

30. Lee J et al. Increased Primary Cilia in Idiopathic Pulmonary Fibrosis. Mol Cells 41, 224–233, doi:10.14348/molcells.2018.2307 (2018). [PubMed: 29477141]

31. Liu L et al. Hedgehog signaling in neonatal and adult lung. Am J Respir Cell Mol Biol 48, 703–710, doi:10.1165/rcmb.2012-0347OC (2013). [PubMed: 23371063]

32. Moshai EF et al. Targeting the hedgehog-glioma-associated oncogene homolog pathway inhibits bleomycin-induced lung fibrosis in mice. Am J Respir Cell Mol Biol 51, 11–25, doi:10.1165/rcmb.2013-0154OC (2014). [PubMed: 24450438]

33. Koli K et al. Bone morphogenetic protein-4 inhibitor gremlin is overexpressed in idiopathic pulmonary fibrosis. Am J Pathol 169, 61–71, doi:10.2353/ajpath.2006.051263 (2006). [PubMed: 16816361]

34. Myllarniemi M et al. Gremlin-mediated decrease in bone morphogenetic protein signaling promotes pulmonary fibrosis. Am J Respir Crit Care Med 177, 321–329, doi:10.1164/rccm.200706-945OC (2008). [PubMed: 17975199]

35. Dong Y et al. Blocking follistatin-like 1 attenuates bleomycin-induced pulmonary fibrosis in mice. J Exp Med 212, 235–252, doi:10.1084/jem.20121878 (2015). [PubMed: 25584011]

References

36. Butler A et al. Integrating single-cell transcriptomic data across different conditions, technologies, and species. Nat Biotechnol 36, 411–420, doi: 10.1038/nbt.4096 (2018). [PubMed: 29608179]

37. Stuart T, et al. Comprehensive Integration of Single-Cell Data. Cell 177, 1888–1902, doi: 10.1016/j.cell.2019.05.031 (2019). [PubMed: 31178118]

38. Finak G, et al. MAST: a flexible statistical framework for assessing transcriptional changes and characterizing heterogeneity in single-cell RNA sequencing data. Genome Biology 16, 278, doi: 10.1186/s13059-015-0844-5 (2015). [PubMed: 26653891]
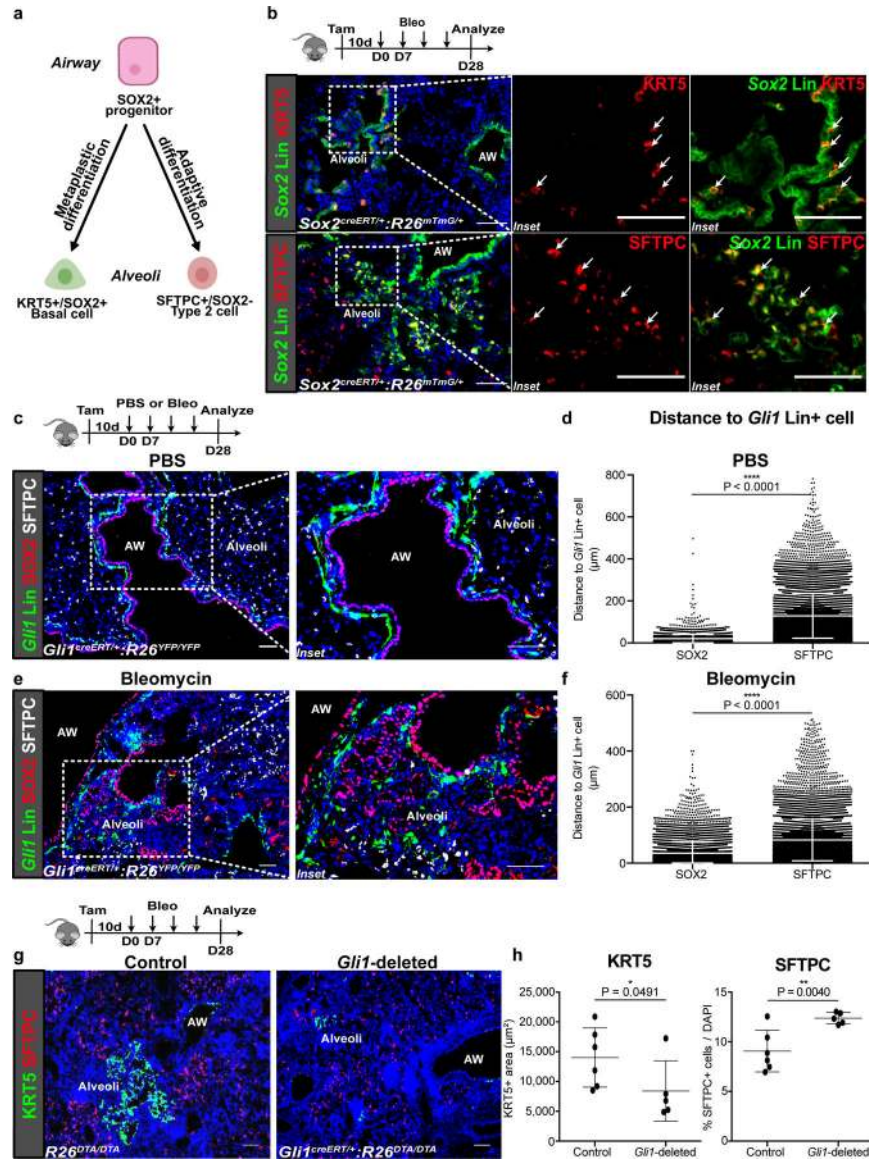
Figure 1. *Gli1*+ mesenchymal cells promote metaplastic KRT5 differentiation *in vivo*.
(**a,b**) Current model of airway progenitors migrating into the alveoli to form endogenous
SFTPC+ Type 2 cells or metaplastic KRT5+ basal cells after severe injury, as demonstrated
by lineage tracing of *Sox2* (*Sox2* Lin+) airway progenitors after repetitive bleomycin
fibrotic injury. This experiment was repeated four times independently with similar results.
(**c,d**) Histology of proximally-located *Gli1*-lineage traced (*Gli1* Lin+) mesenchymal cells
and SOX2+ airway progenitors during homeostasis (PBS treated) with cell-to-cell distance
showing proximity of SOX2+ progenitors and SFTPC+ alveolar progenitors respectively to
Gli1 Lin+ cells during homeostasis (n = 4,207 SOX2 cells, n = 11,945 SFTPC cells; each
datapoint represents an individual distance measurement with all distance measurements for
3 animals plotted; one-tailed unpaired Student's *t*-test). Data are expressed as mean ± SD.
(**e,f**) Histology and average cell-to-cell distance of *Gli1* Lin+ mesenchymal cells in the
alveoli relative to alveolar SOX2+ progenitors during fibrotic repair (n = 7,285 SOX2 cells,

n = 11,710 SFTPC cells; each datapoint represents an individual distance measurement with all distance measurements for 3 animals plotted; one-tailed unpaired Student's *t*-test). Data are expressed as mean ± SD.

(**g,h**) Histology quantification of areas of KRT5+ pods and percentage of SFTPC+ cells after genetic deletion of *Gli1*+ cells with bleomycin injury (n = 6 for control, n = 5 for Gli1-deleted; each data point represents one animal; one-tailed unpaired Student's *t*-test). Data are expressed as mean ± SD. AW = airway. Scale bars, 100 μm.
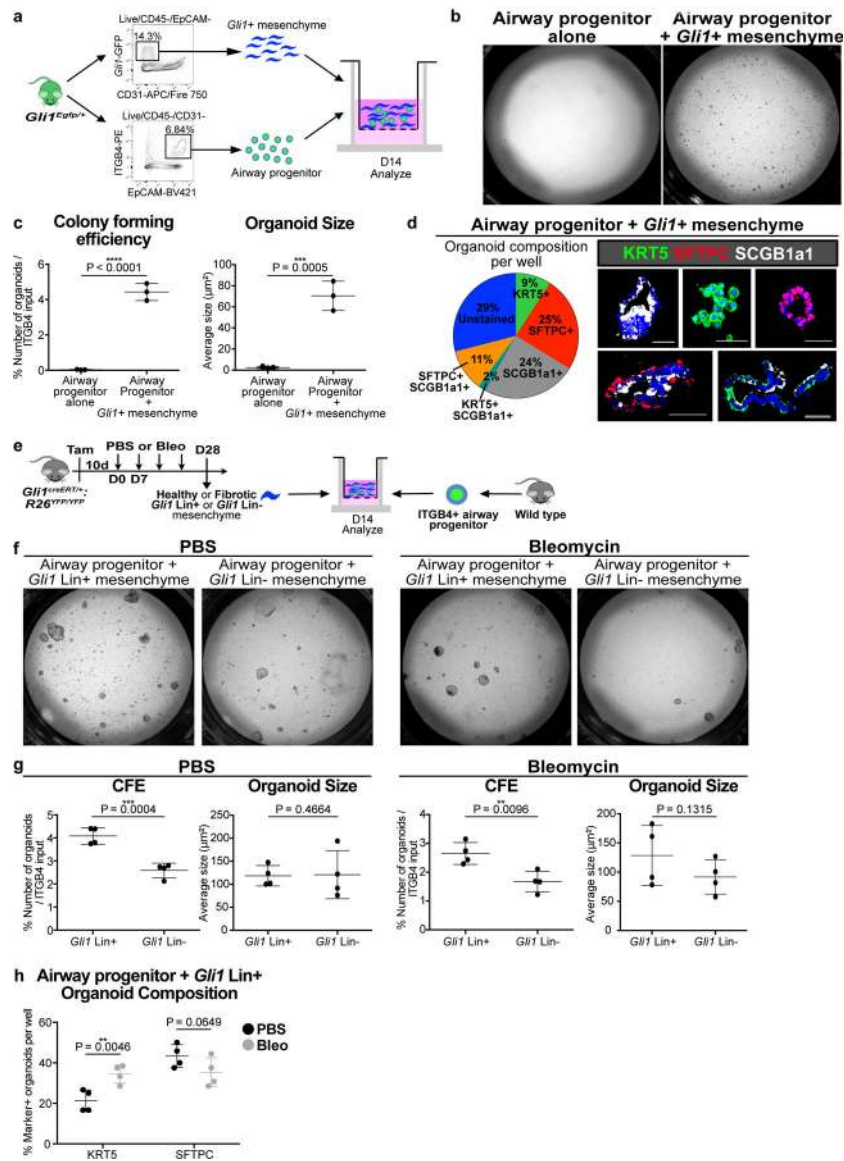
Figure 2. *Gli1+* **mesenchymal cells provide a specialized niche for airway progenitor proliferation and metaplastic differentiation** *in vitro***.**

(**a**) Model of 3D organoid assay of airway progenitor differentiation by co-culturing sorted *Gli1+* cells and ITGB4+ airway progenitors in Matrigel.

(**b,c**) *Gli1+* mesenchyme's effect on airway progenitor growth as demonstrated by colony forming efficiency (CFE) and organoid size of airway progenitor organoids cultured alone or with *Gli1+* mesenchyme (n = 3 per group; each datapoint represents one well; one-tailed unpaired Student's *t*-test). Data are expressed as mean ± SD.

(**d**) Cellular composition of individual airway progenitor-derived organoids.

(**e-g**) CFE of airway progenitors co-cultured with *Gli1* Lin+ or Lin- (CD45-/CD31-/EpCAM-/YFP-) mesenchyme from PBS or bleomycin treated lung (n = 4 per group; each datapoint represents one well; one-tailed unpaired Student's *t*-test). Data are expressed as mean ± SD.

(**h**) Proportion of airway progenitor-derived organoids with KRT5+ basal cells or SFTPC+ type 2 cells co-cultured with *Gli1* Lin+ mesenchyme from bleomycin injured lungs compared to *Gli1* Lin+ mesenchyme from PBS-treated lungs (n = 4 per group; each datapoint represents one well; one-tailed unpaired Student's *t*-test). Data are expressed as mean ± SD. CFE = colony forming efficiency. Scale bars, 100 μm.
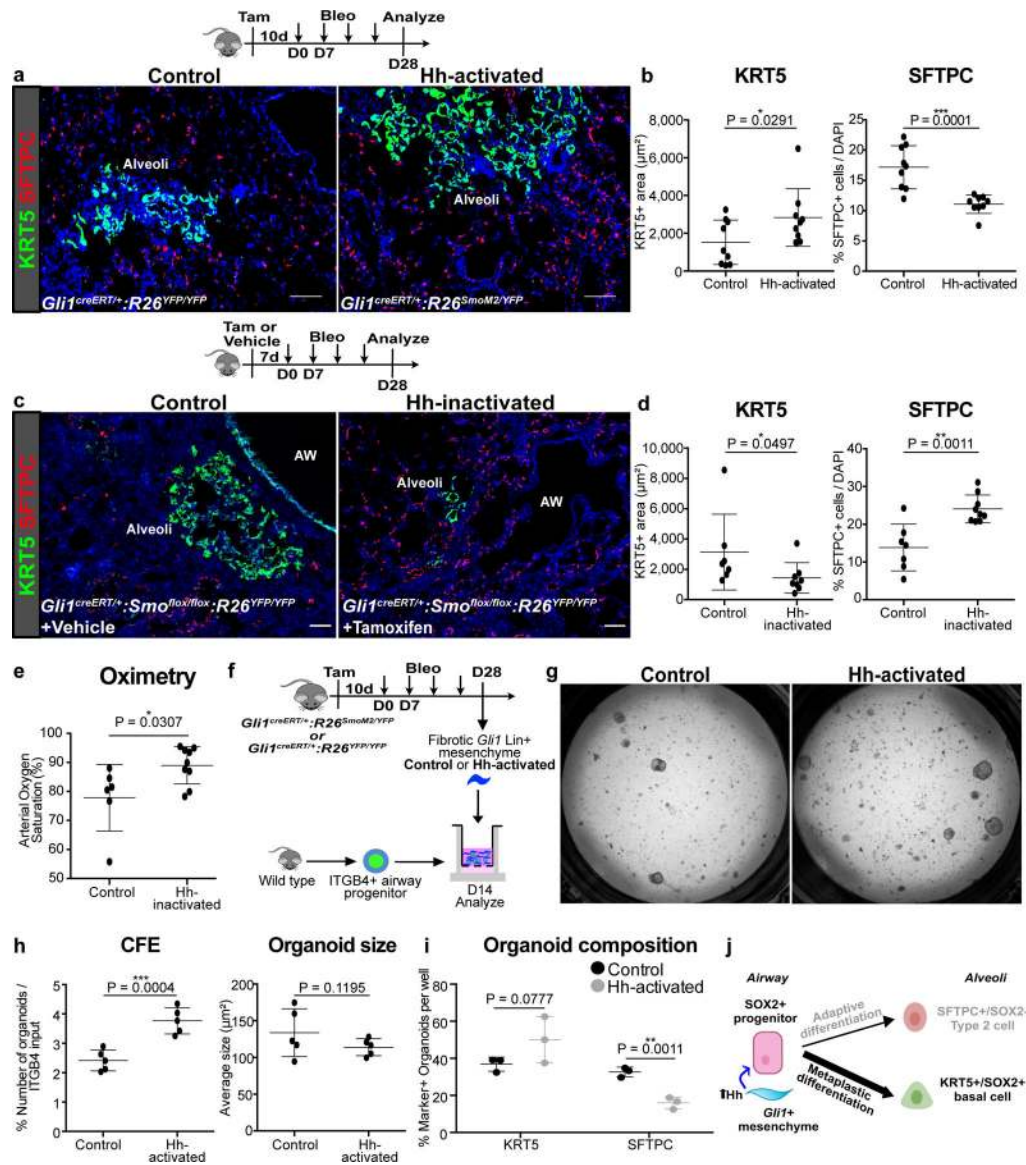
Figure 3. Mesenchymal Hh activation promotes metaplastic KRT5 differentiation while suppressing SFTPC differentiation from airway.

(**a,b**) Histology quantification of areas of KRT5+ pods and percentage of SFTPC+ cells after constitutive Hh activation (activation with *SmoM2*) in *Gli1*+ cells followed by bleomycin injury (n = 9 per group; each data point represents one animal; one-tailed unpaired Student's *t*-test). Data are expressed as mean ± SD.

(**c-e**) Histology quantification of areas of KRT5+ pods and percentage of SFTPC+ cells and oximetry after Hh inactivation (deletion of *Smo*) in *Gli1*+ cells followed by bleomycin injury (n = 7 for control, n = 9 for Hh-inactivated; each data point represents one animal; one-tailed unpaired Student's *t*-test for (d,e)). Data are expressed as mean ± SD.

(**f-i**) CFE, organoid size, and composition of airway progenitors co-cultured with *Gli1* Lin+ mesenchyme isolated from Hh-activated fibrotic lungs compared to *Gli1* Lin+ mesenchyme from control fibrotic lung (n = 5 per group for (h), n = 3 per group for (i); each data point

represents one well; one-tailed unpaired Student's *t*-test for (h,i)). Data are expressed as mean ± SD.

(**j**) Model of Hh activation in the *Gli1*+ mesenchyme acting in trans to promote SOX2+ progenitor differentiation into metaplastic KRT5+ basal cells. Data are expressed as mean ± SD. Hh = hedgehog. Scale bars, 100 μm.
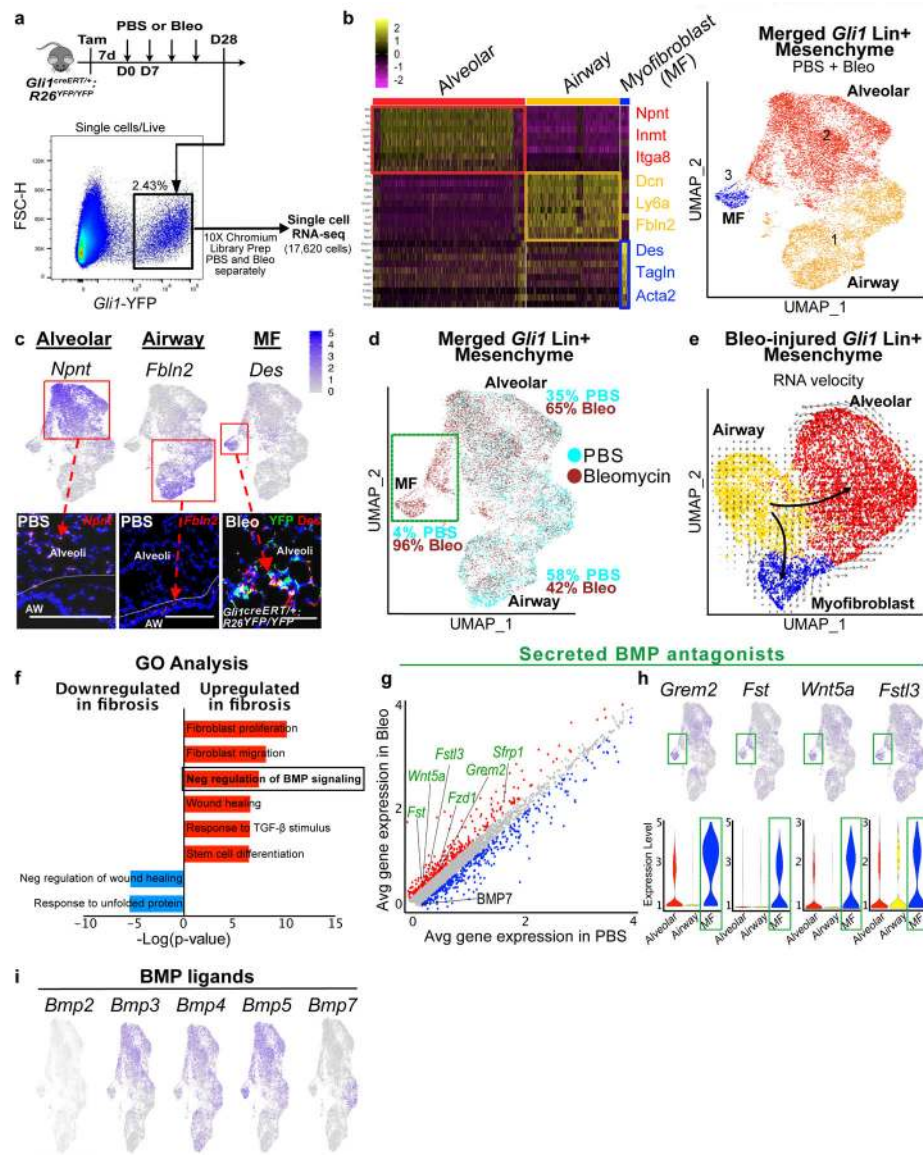
Figure 4. Single cell transcriptome analysis of *Gli1* Lin+ mesenchyme reveals upregulated BMP antagonism in the fibrotic niche.

(**a**) Workflow to isolate *Gli1* Lin+ cells during homeostasis (PBS) and fibrosis (bleomycin) for single cell analysis (one animal per treatment).

(**b**) Left: Heatmap of merged *Gli1* Lin+ cells (PBS and bleomycin) segregates into 3 distinct clusters based on transcriptome, with highest expressing cluster-defining genes to the right. Right: UMAP plot of the three distinct clusters that appears segregated based on anatomic location.

(**c**) *in situ* (RNAscope) and immunofluorescent analysis shows spatial distribution of signature genes for alveolar, airway, and myofibroblast clusters. This experiment was repeated twice independently with similar results.

(**d**) UMAP plot with cells of origin based on treatment shows an increase in proportion of cells in the alveolar and myofibroblast cluster after fibrotic injury. Portion of the alveolar cluster and the entire myofibroblast cluster is derived from bleo-injured cells (green box).

(**e**) RNA velocity analysis predicting the transcriptional trajectory of *Gli1* Lin+ cellular clusters.

(**f**) GO term analysis of differentially-expressed genes between PBS and bleo-treated *Gli1* Lin+ cells reveals enrichment for genes involved in negative regulation of BMP signaling during fibrotic repair (P-adj = 2.26E-02; MAST test).

(**g**) Gene correlation plot with each dot representing a gene, with genes significantly upregulated in fibrotic *Gli1* Lin+ cells in red (P-adj. < 0.1, logfc >0.15) and downregulated (P-adj. < 0.1, logfc <−0.15) in blue. Secreted BMP antagonists (GO term: negative regulation of BMP signaling) are labeled in green (*Grem2* P-adjusted = 1.32E-21; *Fst* P-adj = 2.97E-122; *Wnt5a* P-adj = 2.18E-51; *Sfrp1* P-adj = 2.99E-72; *Fstl3* P-adj = 1.78E-77; *Fzd1* P-adj = 2.36E-69; *Bmp7* P-adj = 8.77E-51; MAST test).

(**h**) Gene feature plots and violin plots of secreted BMP antagonists show enrichment in myofibroblast and part of distal cluster (green box). The violin bodies represent distribution of the cells (n = 11,925 cells).

(**i**) Gene feature plots of BMP ligand expression in *Gli1* Lin+ mesenchyme. MF = myofibroblast, UMAP = Uniform Manifold Approximation and Projection, GO = Gene Ontology, BMP = Bone morphogenetic protein
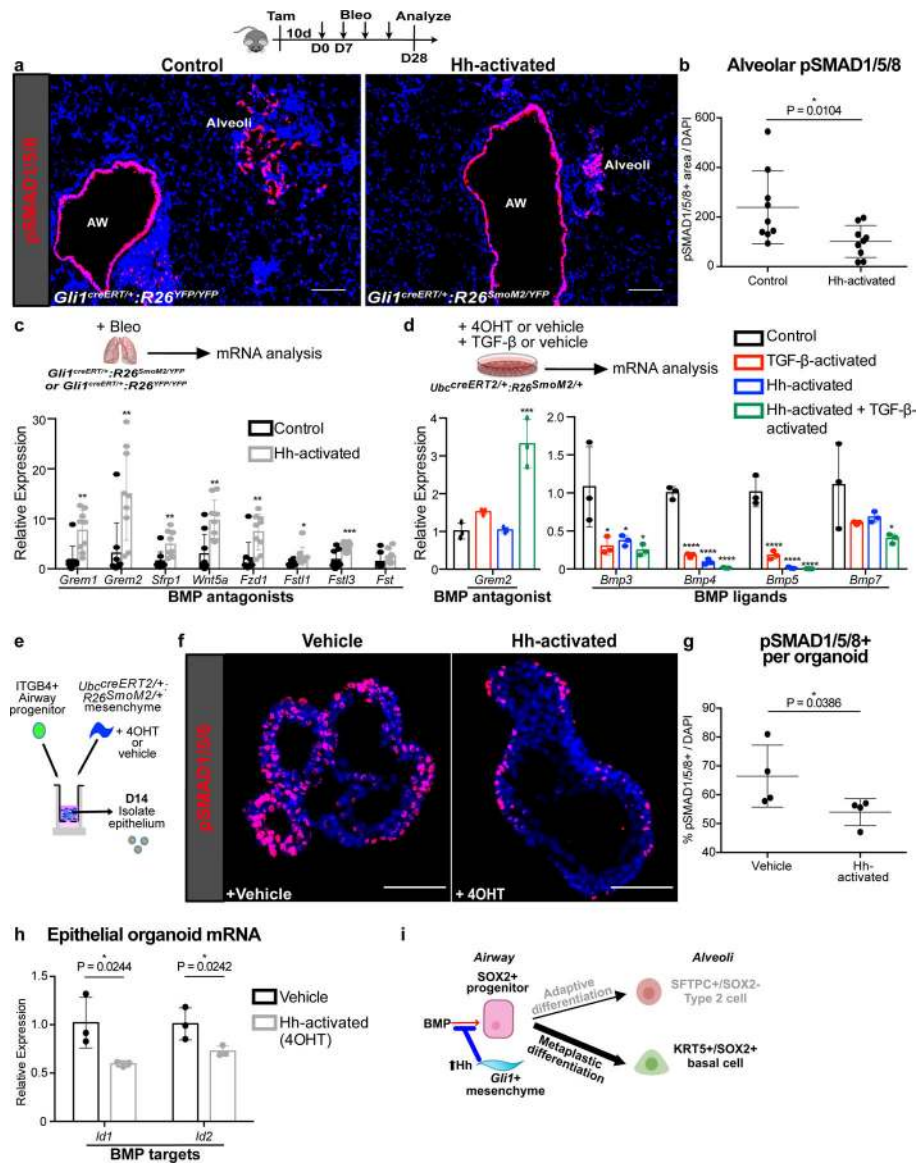
Scale bars, 100 μm.

Figure 5. Hh activation upregulates BMP antagonism in the fibrotic lung.

(**a,b**) Histology quantification of alveolar pSMAD1/5/8 staining in Hh-activated lungs compared to controls in bleomycin treated animals (n = 9 per group; each data point represents one animal; one-tailed unpaired Student's *t*-test). Data are expressed as mean ± SD.

(**c**) Expression of secreted BMP antagonists in Hh-activated lungs compared to controls during fibrotic repair (n = 9 per group; each data point represents one animal; *Grem1* P = 0.0011; *Grem2* P = 0.0027; *Sfrp1* P = 0.0027; *Wnt5a* P = 0.0014; *Fzd1* P = 0.0021; *Fstl1* P = 0.0185; *Fstl3* P = 0.0008; *Fst* P = 0.0686; one-tailed unpaired Student's *t*-test). Data are expressed as mean ± SD.

(**d**) qPCR of BMP antagonist *Grem2* and various BMP ligands in Hh-inducible cultured mesenchyme with or without TGF-β activation (n = 3; each data point represents one biological replicate). *Grem2*: Control v TGF-β P = 0.2431, Control v Hh-activated P =

0.9995, Control v TGF-β + Hh-activated P = 0.0001; *Bmp3*: Control v TGF-β P = 0.0206, Control v Hh-activated P = 0.0330, Control v TGF-β + Hh-activated P = 0.0147; *Bmp4*: Control v TGF-β P < 0.0001, Control v Hh-activated P < 0.0001, Control v TGF-β + Hh-activated P < 0.0001; *Bmp5*: Control v TGF-β P < 0.0001, Control v Hh-activated P < 0.0001, Control v TGF-β + Hh-activated P < 0.0001; *Bmp7*: Control v TGF-β P = 0.1446, Control v Hh-activated P = 0.2303, Control v TGF-β + Hh-activated P = 0.0386; ordinary one-way ANOVA test. Data are expressed as mean ± SD.

(**e-g**) pSMAD1/5/8+ cell number in progenitor-derived organoids with Hh-activated mesenchyme. (n = 4; each data point represents one well; one-tailed unpaired Student's *t*-test). Data are expressed as mean ± SD.

(**h**) BMP target gene expression in epithelial organoids isolated after co-culture with Hh-inducible mesenchyme (n = 3; each datapoint represents one well; one-tailed unpaired Student's *t*-test). Data are expressed as mean ± SD.

(**i**) Hh upregulation of BMP antagonism in the fibrotic progenitor niche drives metaplastic KRT5 differentiation. Scale bars, 100 μm.
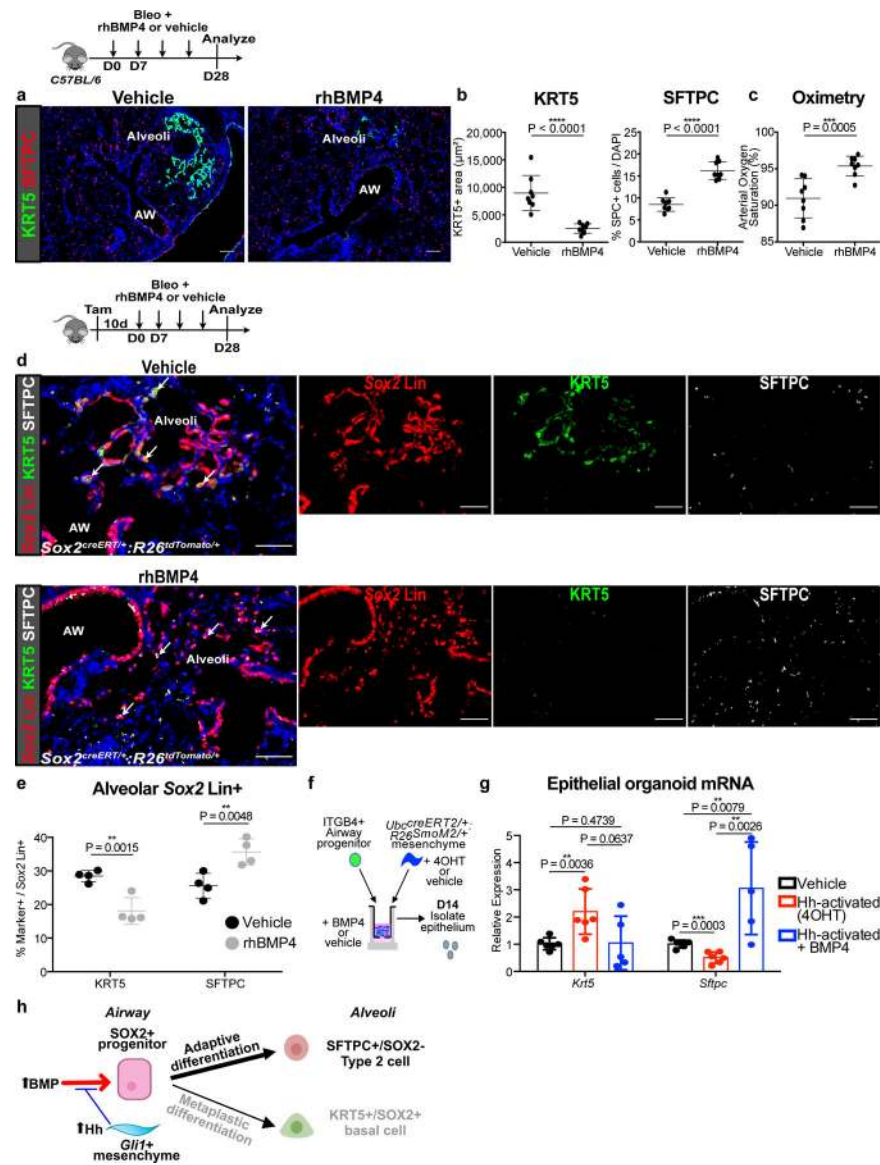
Figure 6. BMP activation attenuates metaplastic airway progenitor differentiation.

(**a-c**) Histology quantification of areas of KRT5+ pods and percentage of SFTPC+ cells and oximetry after addition of rhBMP4 during bleomycin injury (n = 8 per group; each data point represents one animal; one-tailed unpaired Student's *t*-test for (b,c)). Data are expressed as mean ± SD.

(**d,e**) Histologic quantification of alveolar *Sox2* Lin+ cells followed by bleomycin injury and rhBMP4 administration (n = 4 per group; each data point represents one animal; one-tailed unpaired Student's *t*-test). Data are expressed as mean ± SD.

(**f,g**) qPCR of epithelial organoids co-cultured with Hh-activated mesenchyme and rhBMP4. (n = 6 for vehicle, n = 6 for Hh-activated, and n = 5 for Hh-activated + BMP4; each data point represents one well; ordinary one-way ANOVA test). Data are expressed as mean ± SD.

(**h**) Model of BMP activation promoting airway progenitor differentiation into adaptive SFTPC+ Type 2 cells.
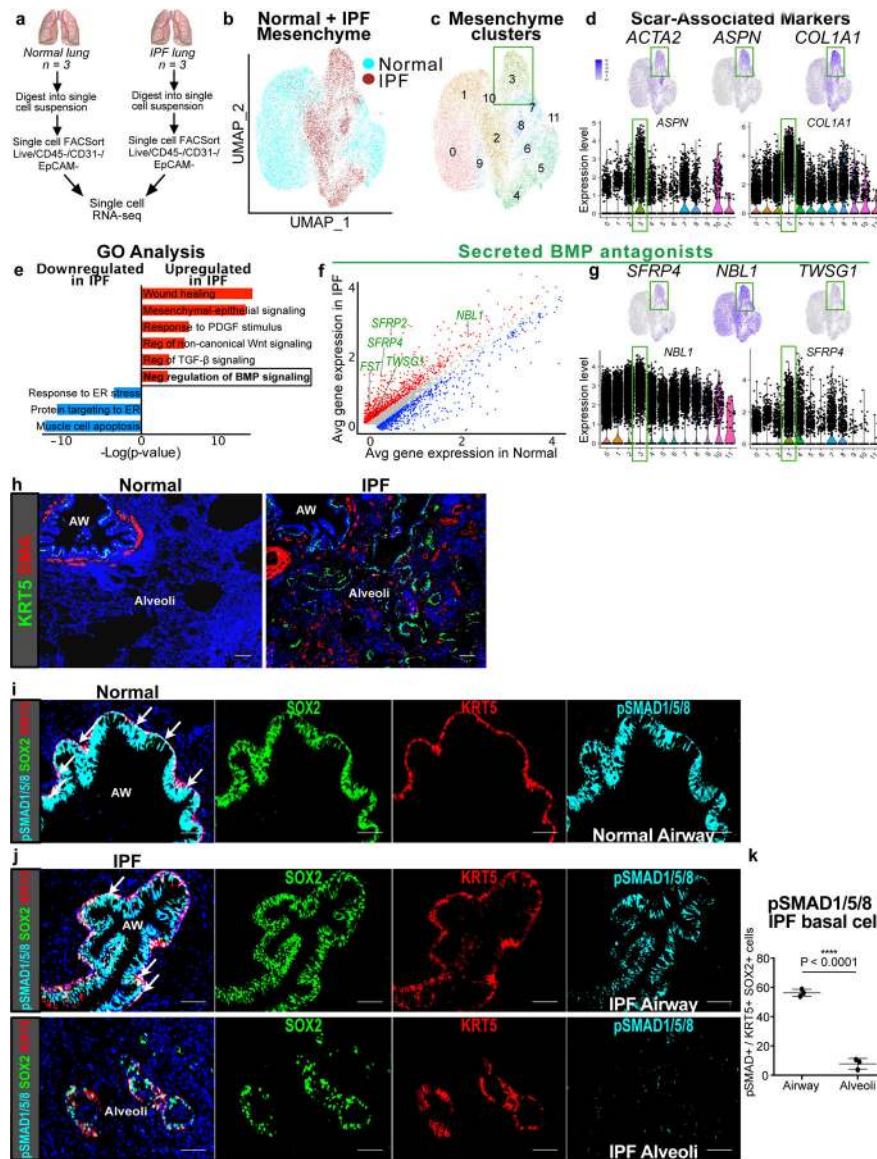
AW = airway, Scale bars, 100 μm.

Figure 7. IPF lungs display altered BMP activation in the epithelium

(**a**) Workflow to isolate mesenchymal cells from explanted IPF lungs and normal donor lungs for single cell RNA-seq analysis (n = 3 per group).

(**b**) UMAP plot with cells of origin based on disease state (IPF vs. normal) shows distinct cellular populations that emerge in the fibrotic state.

(**c,d**) UMAP, gene feature, and violin plots of cluster 3 and scar-associated genes such as myofibroblast differentiation markers, *ACTA2* and *ASPN*, and scar matrix component, *COL1A1*. Each black dot represents one cell. The violin bodies represent distribution of the cells (n = 17,602 cells).

(**e**) GO term analysis of differentially-expressed genes between IPF and normal lung mesenchyme shows enrichment for genes involved in negative regulation of BMP signaling (P-adj = 2.04E-02; MAST test).

(**f**) Gene correlation plot with genes significantly upregulated in IPF in red (P-adj < 0.1, logfc >0.15; MAST test) and downregulated in blue (P-adj < 0.1, logfc <−0.15; MAST test). Secreted BMP antagonists (GO term: negative regulation of BMP signaling) are labeled in green.

(**g**) Expression of BMP antagonists in scar-associated cluster 3.

(**h**) Histology of normal and IPF lungs shows the metaplastic presence of KRT5+ pods and SMA+ fibroblastic foci in the alveoli in IPF. This experiment was repeated independently twice with similar results.

(**i**) pSMAD1/5/8 staining of normal distal airway shows uniform co-localization with SOX2 and KRT5 at the base of the pseudostratified epithelium. This experiment was repeated independently twice with similar results.

(**j**) Top: pSMAD1/5/8 staining of distal airway from IPF lung shows co-localization with SOX2. Bottom: pSMAD1/5/8 staining in the metaplastic SOX2+/KRT5+ basal cells in the alveoli. This experiment was repeated three times independently with similar results.

(**k**) pSMAD1/5/8 staining in the alveolar SOX2+/KRT5+ basal cells relative to their airway counterpart in IPF lungs (n = 3 samples; same sample was analyzed in the airway and alveolar region; one-tailed unpaired Student's *t*-test). Data are expressed as mean ± SD. Scale bars, 100 μm.